Thermal and Rheological Structure of Lithosphere beneath Northeast China

Dong Yan[1], You Tian[1], Dapeng Zhao[2], and Hongli Li[1]

[1]Jilin University
[2]Tohoku University

November 24, 2022

Abstract

We investigate the 3-D lithospheric thermal and rheological structures beneath Northeast China using detailed P- and S-wave velocity models following mineral physics as well as geothermal methods. Small-scale temperature changes and thermal lithosphere thickness variations between different tectonic blocks are revealed. Our results show that strong lateral heterogeneities exist in the lithospheric thermal structure and rheological structure on both sides of the North-South Gravity Lineament (NSGL). The Changbai volcanic area and the central part of the Songliao Basin in the eastern side of the NSGL exhibit higher temperatures, thinner thermal lithosphere and lower rheological strength, which are closely associated with the western Pacific plate subduction under the Eurasian continent, resulting in upwelling of wet and hot asthenospheric material above the stagnant Pacific slab in the mantle transition zone. The thermo-chemical erosion of the upwelling asthenospheric material may induce delamination of partial lithosphere under the Songliao Basin. In addition, the Songliao Basin edge is characterized by lower temperature, thicker thermal lithosphere and higher rheological strength, which may indicate a relatively stable lithosphere. The Halaha and Abaga volcanic areas in the western side of the NSGL exhibit higher temperature, thinner thermal lithosphere and lower rheological strength, which could be caused by small-scale upwelling of hot asthenospheric material associated with delamination of partial lithosphere beneath the Songliao Basin.

Thermal and Rheological Structure of Lithosphere beneath Northeast China

Dong Yan[1], You Tian[1,2*], Dapeng Zhao[3], Hongli Li[1]

1. College of Geoexploration Science and Technology, Jilin University, Changchun 130026, China
2. Changbai Volcano Geophysical Observatory, Ministry of Education, Changchun 130026, China
3. Department of Geophysics, Graduate School of Science, Tohoku University, Sendai 980-8578, Japan

Corresponding author: You Tian (tianyou@jlu.edu.cn)

Key Points:

- A 3-D model of lithospheric thermal structure and rheological strength beneath Northeast China is presented.
- Small-scale temperature changes and thermal lithosphere thickness variations between different tectonic blocks are revealed.
- The “crème brûlée” model can explain the lithospheric deformation in Northeast China.

Abstract

We investigate the 3-D lithospheric thermal and rheological structures beneath Northeast China using detailed P- and S-wave velocity models following mineral physics as well as geothermal methods. Small-scale temperature changes and thermal lithosphere thickness variations between different tectonic blocks are revealed. Our results show that strong lateral heterogeneities exist in the lithospheric thermal structure and rheological structure on both sides of the North-South Gravity Lineament (NSGL). The Changbai volcanic area and the central part of the Songliao

Basin in the eastern side of the NSGL exhibit higher temperatures, thinner thermal lithosphere and lower rheological strength, which are closely associated with the western Pacific plate subduction under the Eurasian continent, resulting in upwelling of wet and hot asthenospheric material above the stagnant Pacific slab in the mantle transition zone. The thermo-chemical erosion of the upwelling asthenospheric material may induce delamination of partial lithosphere under the Songliao Basin. In addition, the Songliao Basin edge is characterized by lower temperature, thicker thermal lithosphere and higher rheological strength, which may indicate a relatively stable lithosphere. The Halaha and Abaga volcanic areas in the western side of the NSGL exhibit higher temperature, thinner thermal lithosphere and lower rheological strength, which could be caused by small-scale upwelling of hot asthenospheric material associated with delamination of partial lithosphere beneath the Songliao Basin.

Plain Language Summary

We determine a 3-D model of lithospheric thermal and rheological structure under Northeast China to better understand the lithospheric destruction mechanism. Small-scale thermal and rheological structures between different tectonic blocks are revealed. There are significant lateral differences in the 3-D model between two sides of the North-South Gravity Lineament (NSGL), which serves as a vital tectonic boundary in eastern China. In the east of the NSGL, the Changbai volcano and the central part of the Songliao Basin show higher temperatures, thinner thermal lithosphere and lower rheological strength, which may be associated with upwelling of wet and hot asthenospheric material induced by the western Pacific plate subduction under the Eurasian plate. The thermo-chemical erosion of the ascending asthenospheric material could induce partial lithosphere beneath the Songliao Basin to sink into the upper mantle, leading to small-scale upwelling of asthenospheric material and providing magmas to the Halaha and Abaga volcanoes in the west of the NSGL. The edge of the Songliao Basin exhibits lower temperature, thicker thermal lithosphere and higher rheological strength, which may indicate a relatively stable

lithosphere.

1. Introduction

Northeast China is situated between the Sino-Korean Craton and the Siberian Plateau, facing the Japan Sea to the east (Figure 1). It is generally believed that in the early Mesozoic, Northeast China collided with North China along the Solonker suture zone (Sengor et al., 1993). During the late Mesozoic to Cenozoic, extensional structures had been widely developed in eastern China due to the combined effects of the Mongolia-Okhotsk Ocean closure and the westward subduction of the Pacific plate (Wang et al., 2006; Xu et al., 2013; Guo et al., 2018), which contributed to the formation of widespread extensional basins and orogenic belts, resulting in the nearly NE- and NNE-trending tectonic patterns of Northeast China at present (Figure 1).

The complex tectonic pattern of Northeast China has been extensively investigated in the past decades, and researchers have proposed several mechanisms to explain its tectonic evolution. Some workers have suggested that the widespread tectonic deformation and lithospheric thinning of Northeast China are associated with the western Pacific plate subduction or the closure of the Okhotsk Ocean (e.g., Ren et al., 2002; Meng et al., 2003; Zhao et al., 2004). A few other studies have shown that the subduction of the Pacific plate and the Philippine Sea plate contributed to the formation and development of the western Pacific marginal basins and Mesozoic basins in eastern China, resulting in strong lateral heterogeneity in the lithosphere (Li et al., 2012; Li et al., 2013). Xu et al. (2013) suggested that the tectonic evolution of Northeast China was mainly affected by the closure of the Mongolia-Okhotsk Ocean from the Jurassic to early Cretaceous, whereas the strong volcanic activities during the late Cretaceous were primarily related to the Paleo-Pacific plate subduction.

Many previous studies have investigated the seismic velocity structure beneath Northeast China (e.g., Pan et al., 2014; Guo et al., 2016; Kang et al., 2016; Tian et al., 2017; Guo et al., 2018; Ma et al., 2018; Tian et al., 2019; Jia et al., 2022), but there have been few studies of the thermal and rheological structure beneath this region. The study on the lithospheric thermal structure is mainly about the lithospheric temperature distribution as well as variations of the thermal lithosphere thickness, and the lithospheric rheological structure is mainly described by two recognized rheological models: the jelly sandwich model (Ranalli & Murphy, 1987) and the crème brulée model (Jackson, 2002). The conventional jelly sandwich model is based on rock mechanics results, suggesting that a weak ductile layer at the bottom of the lower crust separates the relatively strong upper crust and the uppermost mantle. In addition, the uppermost mantle contributes most to the lithospheric strength. This prevailing model had been used for almost two decades before the crème brûlée model was put forward. The new model is based on the depth distribution of seismicity, suggesting that a relatively strong crust underlain by a weak mantle and continental tectonic activities are controlled by the strength that is primarily distributed in the crust.

An and Shi (2006) studied the 3-D temperature structure at depths of 70-240 km beneath Mainland China using a shear wave velocity (Vs) model (CN03S) and estimated the thermal lithosphere thickness by considering the mantle adiabatic temperature at 1300℃. Sun et al. (2013) investigated the lithospheric temperature structure beneath the Chinese continent by solving the 3-D steady-state heat conduction equation using the finite element simulation. Deng and Tesauro (2016) investigated the thermal structure of the Chinese continental lithosphere by using the crustal temperature model of Sun et al. (2013) and the Vs model of Li et al. (2013). As a result, Deng and Tesauro (2016) obtained a lithospheric strength model of Mainland China. Although these previous studies have addressed the thermal and rheological structure of some representative tectonic blocks, their results could not reveal small-scale lateral variations of the lithospheric temperature and rheological strength under Northeast China due to the limited resolution of the previous models.

It is well recognized that temperature is a critical parameter in geodynamic studies because geodynamic and rheological processes in the mantle are mainly controlled by temperature (An & Shi, 2006, 2007). Furthermore, rheological properties of the lithosphere play an important role in controlling the tectonic deformation and geological evolution processes (Burov, 2011; Ranalli & Adams, 2013). Therefore, it is of great significance to clarify the spatial variation of lithospheric thermal structure and rheological strength beneath Northeast China to better understand its lithospheric deformation, intraplate volcanism and mantle dynamics.

In this work, we determine a new 3-D model of lithospheric thermal structure and rheological strength beneath Northeast China, which reveals many small-scale features of lithospheric structure of the region. The thermal lithosphere thickness in this region is determined from the 1300℃ isotherm of the mantle adiabatic temperature. In addition, we analyze the relationship between the lithospheric strength and seismicity of the study region. The present results provide new constraints on the tectonic evolution process as well as the destruction mechanism of the continental lithosphere under Northeast China.

2. Geological and Tectonic Settings

Northeast China is bounded in the south by the Solonker suture zone, and in the north by the Mongolia-Okhotsk suture zone. Northeast China consists of several continental microplates, including the Erguna block and Xing'an block in the west, the Jiamusi block in the east, and the Songliao block in the middle (Wu et al., 1995; Zhou & Wilde, 2013; Zhang et al., 2014). The Xing'an block primarily consists of the Great Xing'an Range where widespread late Mesozoic volcanic rocks exist (Xu et al., 2013). The Songliao block is mainly composed of the Great and Lesser Xing’an Ranges in the southwest and northeast, respectively, the Songliao Basin in the center and the Zhangguangcai Range in the east (Wang & Li, 2018). In the late Mesozoic, the western Pacific plate subduction led to the accretion of the Nadanhada Terrane and the Jiamusi Block along the East Asian continental margin. During this period the crustal deformation is characterized by the formation of some NNE-trending faults in parallel with the continental margin. One of the major faults is the Tanlu fault zone, which branches into the Yilan-Yitong fault and the Dunhua-Mishan fault. The Yilan-Yitong fault has developed as an internal fault in the Songnen-Zhangguangcai Range Massif, separating the Songliao Basin and the Zhangguangcai Range. The Dunhua-Mishan fault has served as a tectonic boundary between the Nadanhada Terrane and the Xingkai Massif (Xu et al., 2017).

During the late Mesozoic to Cenozoic, widespread tectonic deformations occurred in Northeast China, resulting in lithospheric thinning and intensive magmatic activities. In addition, widespread rifting and extensional basins have formed along the large-scale strike-slip faults (Griffin et al., 1998; Ren et al., 2002; Zhu et al., 2011; Zhang et al., 2014), including the Erlian Basin, the Hailar Basin and the Songliao Basin, which are mostly filled with several kilometers of lacustrine sediments. The Songliao Basin is the largest and an oil-producing basin, which has made prominent contributions to the oil and gas production for decades (Wang et al., 2001).

The Songliao Basin has a typical double-base structure. Its lower base is composed of late Jurassic and early Cretaceous rifting basins, which were filled with pyroclastic rocks and lacustrine sediments. Its upper base consists of widespread depressions, in which the lacustrine and delta sedimentary systems were formed during the late Cretaceous, and alluvial fans as well as fluvial strata were deposited during the Eocene and Neogene (Ren et al., 2002). Cenozoic volcanic rocks are distributed extensively in the rift valleys and ridges at edges of the Songliao Basin (Liu et al., 2001). Some of the best-known volcanic centers in Northeast China include the Changbai, Longgang, Jingpohu and Wudalianchi volcanoes (Figure 1). Therefore, Northeast China is an ideal natural laboratory to investigate the Cenozoic intraplate volcanism.

The North-South Gravity Lineament (NSGL), extending more than 3500 km from Northeast China to South China, serves as a vital tectonic boundary within mainland China (Figure 1). This lineament is generally parallel to the Tanlu fault zone and it passes through many important tectonic units in eastern China, including the NCC, the Dabie orogen, and the Yanshan orogen. The surface topography, the thicknesses of the crust and lithosphere, and the Bouguer gravity anomalies all change dramatically across the NSGL, indicating that it is an important physical boundary in eastern China (Menzies & Xu, 1998; Niu, 2005). Analysis of Sr-Nd-Os isotope data for mantle xenoliths extracted from two sides of the NSGL show that it is also a geochemical boundary that separates two distinct mantle domains formed in different geological periods (Xu, 2007). Yang et al. (2005) investigated the crustal and lithospheric geophysical characteristics on both sides of the NSGL using seven geoscience transects. They suggested that the interactions of the Eurasian plate, the Indian plate and the Pacific plate, as well as mantle flow at the East Asian continent margin contributed to the crust-mantle structure on both sides of the gravity lineament. Xu (2007) suggested that the western Pacific plate subduction under the Eurasian continent has caused the lithospheric thinning with varying degrees beneath the western and eastern NCC, which may be a critical factor in the formation of the NSGL. In addition, the upwelling of asthenospheric material induced by dehydration of the stagnant Pacific slab in the mantle transition zone may further accelerate the formation of the NSGL (e.g., Zhao et al., 2004, 2009; Lei & Zhao, 2005; Huang & Zhao, 2006; Tian et al., 2009; Xu & Zhao, 2009). However, there is still no consensus on the formation mechanism of the NSGL to date. Therefore, it is of great significance to get further insight into the geophysical characteristics on both sides of the NSGL in Northeast China to better understand its formation and tectonic evolution mechanism.

3. Data and Method

3.1. Seismic Velocity Models

The temperature distribution of the lithosphere is commonly estimated by solving the heat conduction equation with heat flow data, because heat conduction is the major transmission mode of thermal energy in the lithosphere. A number of geothermal studies have been made for North China (e.g., Zang et al., 2002a; He, 2014; Huang et al., 2015; Zhang et al., 2016). However, the scarcity and uncertainty of heat flow data in Northeast China have hindered the estimation of lithospheric temperature distribution. In the present work, we study the 3-D temperature structure of the upper mantle at depths of 50-200 km beneath Northeast China using the robust 3-D P- and S-wave velocity (Vp, Vs) models of Ma et al. (2018) and Shen et al. (2016) (see Figures S1 and S2 in Supporting Information) following a mineral physics approach (Goes et al., 2000; Deschamps et al., 2002; An & Shi, 2006; Yang et al., 2013; Yan et al., 2019), which is described in detail in the Appendix.

The 3-D Vp model was determined by applying the joint inversion method of Zhao et al. (1992, 1994) to a great number of arrival-time data of local and regional earthquakes as well as relative travel-time residuals of teleseismic events (Ma et al., 2018). A 3-D ray-tracing technique by Zhao et al. (1992) was used to calculate theoretical travel times and ray paths. Depth variations of the Moho discontinuity were taken into account to improve the computing accuracy. The LSQR algorithm of Paige & Saunders (1982) was used to solve the large but sparse system of observation equations. Resolution tests showed that the lateral resolution of the 3-D Vp model is ~100 km beneath most parts of the study region.

The 3-D Vs model was obtained by ambient noise Rayleigh wave tomography using data recorded at 2073 seismic stations of multiple networks in China and earthquake surface wave tomography beneath the NECESS array in Northeast China (Shen et al., 2016). The same quality control procedures were applied to all data. The 3-D Vs model was produced by a Bayesian Monte Carlo inversion on a 0.5°×0.5° grid across the study region.

The high-resolution 3-D Vp and Vs models show similar velocity anomaly patterns except beneath some areas of the Erguna block where the distribution of seismic stations is sparse. Many significant tectonic and geological features in the lithosphere beneath Northeast China are revealed by the Vp and Vs models (Figure S1 and Figure S2). In the western side of the NSGL, some low-Vp and low-Vs anomalies exist beneath the Halaha and Abaga volcanic areas. In the eastern side of the NSGL, prominent low-Vp and low-Vs zones at depths of 50-200 km are visible beneath the Cenozoic volcanic areas such as Changbai, Longgang and Jingpohu, which are in good agreement with many previous tomographic results (e.g., Zhao et al., 2004, 2009; Zhao & Tian, 2013; Tian et al., 2016, 2019; Guo et al., 2016, 2018). Significant high-Vp and high-Vs anomalies appear at edges of the Songliao Basin, and low-Vp and low-Vs anomalies are visible under the central part of the Songliao Basin, which are consistent with the previous seismic results (e.g., Guo et al., 2016, 2018).

3.2. Lithospheric Temperature Estimation

We adopt the high-resolution 3-D Vp and Vs models described above and use a global enumeration algorithm to invert seismic velocities for 3-D temperature structure of the upper mantle at depths of 50-200 km. To obtain a more accurate inversion result, we conduct a joint inversion of the Vp and Vs models to constrain the 3-D temperature structure of the upper mantle beneath Northeast China. The average annual surface temperature (~10℃) and the inverted temperature values at 50 km depth are adopted as the top and bottom boundary conditions, respectively, and the lithospheric temperature distribution above this depth (50 km) is estimated by solving the 1-D steady-state heat conduction equation. The sedimentary layer is not taken into account in our stratified crust model, because the average sediment thickness in Northeast China is less than 1 km according to the CRUST 1.0 model (https://igppweb.ucsd.edu/~gabi/crust1.html) and some previous studies (Laske et al., 2013; Tao et al., 2014). The stratified crust model is built with Vp < 6.2 km/s for the upper crust, and for the middle crust with Vp of 6.2-6.5 km/s. The bottom boundary of the crust is determined by referring to the receiver function results of Zhang et al. (2020) and the CRUST 1.0 model.

The thermal conductivity is taken as $k = k_0(1 + cz)(1 + b(T - 273.15))^{-1}$ in the crust (Chapman, 1986) and $k = 0.368 \times 10^{-9} \times T^3 + (0.174 + 0.000265 \times T)^{-1}$ in the lithospheric mantle (Doin & Fleitout, 1996). Here k_0 is measured thermal conductivity at zero temperature and one atmosphere pressure, which is assumed to be 3.0, 2.8 and 2.6 $W \cdot m^{-1} \cdot K^{-1}$ for the upper, middle and lower crust, respectively. The temperature coefficient b is taken as 1.5×10^{-3}, 0.8×10^{-4} and 1.5×10^{-4} K^{-1} for the upper, middle and lower crust, respectively. The pressure coefficient c is equal to 1.5×10^{-3} km^{-1} for the whole crust. T is temperature (in Kelvin) at a depth of z (in km)

The heat production distribution in a stratified crust model is obtained by using the empirical relationship between P-wave velocity (V_P^0) and the heat production (A) proposed by Rybach & Buntebarth (1984):

$$\ln A = 13.7 - 2.17 V_P^0 \quad (293.15\ \mathrm{K},\ 100\ \mathrm{MPa}) \tag{1}$$

It is an effective method to estimate the heat production when heat flow data and radioactive element abundance data are sparse in a study region. However, the V_P in the deep earth is the in-situ velocity, which could considerably differ from the laboratory condition. Thus, it has to be corrected to the experimental reference conditions (293.15 K, 100 MPa) according to the following formula (Rybach and Buntebarth, 1984; Sun et al., 2013):

$$V_P^0 = V_P + (293.15 - T)\frac{\partial V_P}{\partial T} + (100 - P)\frac{\partial V_P}{\partial P} \tag{2}$$

where V_P is P-wave velocity at specific temperature T and pressure P (assumed to be lithostatic pressure). The temperature and pressure derivatives for each layer of the stratified crust model are listed in Table S1 in the Supporting Information. Nevertheless, the calculated heat production is high beneath some areas in the shallow part of the upper crust due to the low V_P, thus it is more appropriate to consider the heat production within the upper crust as a constant, which is assumed to be 1.25 $\mu W \cdot m^{-3}$ in this study (Chi & Yan, 1998; Zang et al., 2002a). For the lithospheric mantle, a uniform heat production of 0.03 $\mu W \cdot m^{-3}$ is adopted (Rudnick et al, 1998; Wang, 2001).

3.3. Lithospheric Strength Estimation

The rheological structure of the lithosphere changes in space and time as a function of diverse factors, in particular, temperature, rock compositions, and pore fluid pressure (Ranalli, 2000). There are three main mechanisms for the lithospheric rheology, i.e., frictional sliding, brittle fracture and ductile creep (Kirby, 1983; Kohlstedt et al., 1995; Zang et al., 2007). Some previous studies have shown that in the shallow parts of the lithosphere with a low temperature, the dominant mechanism is the rock brittle deformation (frictional sliding and brittle fracture), whereas at greater depths with a high temperature, rocks predominantly deform by the ductile creep mechanism (Tesauro et al., 2012, 2015). In addition, frictional sliding mainly occurs in the upper crust, whereas brittle fracture takes place primarily in the lower crust and the uppermost mantle (Zang et al., 2007).

Frictional sliding depends linearly on pressure, which is independent of temperature and strain rate (Pauselli et al., 2010). The Byerlee's law is widely accepted as the criterion for describing the frictional sliding along brittle faults in the crust, because the law was proposed based on experimental data (Byerlee, 1978), which can be expressed as:

$$\sigma_f = f\rho g z(1-\lambda) \tag{3}$$

where f is a numerical factor related to the fault type, being 3.0, 1.2 and 0.75 for thrust faulting, strike-slip faulting and normal faulting, respectively. ρ represents the average density of rocks above depth z, g is the acceleration due to gravity, and λ is the pore fluid factor (ratio of pore fluid pressure to lithostatic pressure). In this study, we use the frictional sliding formula under the strike-slip faulting condition ($f = 1.2$) to calculate the lithospheric strength, because the faults in Northeast China are dominated by NNE-trending strike-slip motions (Ren et al., 2002; Xu et al., 2017).

However, in most of the previous studies, only the frictional sliding and ductile creep mechanisms were considered, whereas the brittle fracture was ignored because there was no appropriate way to do that, leading to an increase in the magnitude of rheological strength calculated. In this study, we take the brittle fracture mechanism into consideration in the process of calculating the rock strength in the lithosphere according to the empirical formula given by Zang et al. (2007):

$$\sigma_b = B_0\left[1+K\left(\frac{\sigma_c}{B_0}\right)^m\right]\left[1+\alpha\left(\lg\frac{T}{T_0}\right)^\beta\right]\left[1+\gamma\lg\left(\frac{\dot{\varepsilon}}{\dot{\varepsilon}_0}\right)\right] \tag{4}$$

where B_0, K, m, α, β and γ are empirical failure parameters that are listed in Table S2, σ_c denotes confining pressure that equals to lithostatic pressure, T is the temperature in Kelvin, T_0 is the room temperature (298.15 K), $\dot{\varepsilon}$ and $\dot{\varepsilon}_0$ (10^{-5} s^{-1}) are strain rate and reference strain rate, respectively. Previous studies have suggested that there is little difference in the rheological strength obtained by using the constant strain rate and observed strain rate from GPS observations (Zang et al., 2005; Tesauro et al., 2015; Deng & Tesauro, 2016). In this study, we calculate the lithospheric strength using the global average strain rate of 10^{-15} s^{-1}.

The creep strength of the lithosphere is generally described by power law (Weertman, 1970; Kohlstedt et al., 1995). We can calculate the lithospheric creep strength according to the following equation:

$$\sigma_d = \left(\frac{\dot{\varepsilon}}{C}\right)^{\frac{1}{n}} exp\left(\frac{Q}{nRT}\right) \tag{5}$$

where $\dot{\varepsilon}$ is the strain rate, C, n and Q are material creep parameters independent of temperature and pressure, which represent the flow parameter, stress exponent and activation enthalpy, respectively, R is the gas constant, and T is the temperature in Kelvin. Previous studies have shown that the lithospheric rheological models can be divided into the soft rheology model and the hard rheology model according to the rock composition (Ranalli, 2000; Pauselli et al., 2010; Deng & Tesauro, 2016). A soft rheology is assumed to be controlled by felsic granulite and wet peridotite in the lower crust and the lithospheric mantle, respectively, whereas a hard rheology is controlled by mafic granulite and dry peridotite in the lower crust and the lithospheric mantle, respectively (Pauselli et al., 2010). Furthermore, a wet lithospheric mantle model is more suitable for areas that have been influenced recently by oceanic plate subduction and tectonic thermal events, whereas a dry lithospheric mantle might be more relevant for old and stable regions (Afonso & Ranalli, 2004). Northeast China has experienced multi-stage tectonic thermal events since the late Mesozoic to the Cenozoic. Hence, it is more suitable to choose the soft rheological model to study the lithospheric strength of Northeast China. The rheological parameters for lithospheric materials in this study are listed in Table S3.

In any depth range, rocks tend to deform by the dominant mechanism that exhibits the lowest strength (Kirby et al., 1991, 1996; Zang et al., 2007), and the rheological strength of the lithosphere at a specific depth is generally described by the yield strength envelop (YSE), which describes the maximum rock strength as a function of depth (Goetze & Evans, 1979). The integrated lithospheric strength (σ_L) is estimated by vertical integration of the YSE as follows:

$$\sigma_L = \int_0^H \mathrm{YSE}\, dz \tag{6}$$

where H is the lithospheric thickness, and z is depth.

4. Results and Discussion

4.1. Lithospheric Temperature Structure

In this study, we investigate the 3-D temperature (T) structure of the upper mantle at depths of 50-200 km from the Vp and Vs models described in Section 3.1 (Figure S3 and Figure S4). The T distributions estimated from the separate Vp and Vs models are similar to each other. Significant low-T zones exist beneath the Cenozoic volcanic areas. The edge of the Songliao Basin generally exhibits prominent low-T zones, and a relatively high-T zone appears under the central part of the Songliao Basin. The T distribution exhibits obvious differences in some areas of the Erguna block, which may be related to the discrepancy of Vp and Vs models due to the sparse distribution of seismic stations there. Figure 2 shows map views of the 3-D T structure obtained from the Vp and Vs joint inversion. Figure 3 shows eight vertical cross-sections of the 3-D lithospheric temperature model. The lithospheric temperature distribution above 50 km depth obtained by solving the 1-D steady-state heat conduction equation is displayed more clearly in Figure 4.

Our results reveal strong lateral heterogeneities in the lithospheric mantle beneath Northeast China. Significant high-T zones are visible at 50-200 km depths beneath the Halaha and Abaga volcanic areas in the western side of the NSGL (Figures 2, 3b, 3f and 3g). The two areas are characterized by relatively high-T zones in the middle and lower crust as well (Figures 4b, 4f and 4g). Some high-T zones exist beneath the Hailar Basin and the Erlian Basin (Figures 2c-2f, 3d and 3h). In the eastern side of the NSGL, prominent high-T zones exist at depths of 50-200 km beneath the Cenozoic volcanic areas such as Changbai, Longgang and Jingpohu (Figures 2, 3a-3c). Significant low-T zones appear at the edge of the Songliao Basin, and a prominent high-T zone is visible under the central part of the Songliao Basin (Figures 2, 3d and 3e), which accord with the previous results obtained from other geophysical observations. For instance, surface heat flow data show that the central part of the Songliao Basin exhibits higher heat flow values and higher geothermal gradients (Wang, 2001; Wang & Cheng, 2011; Jiang et al., 2016). MT observations revealed prominent low-resistivity anomalies in the lithospheric mantle beneath the Changbai Volcano and the Songliao Basin (Han et al., 2018; Li et al., 2020). Significant high-T anomalies are visible beneath the Tanlu fault zone and the Sanjiang Basin (Figure 2 and Figure 3d-3f). The major geological tectonic units in Northeast China exhibit a NE-SW to NNE-SSW trending pattern, and the temperature anomalies in our results are generally consistent with this tectonic trend. Our results reveal some small-scale features of temperature variations between different tectonic blocks, as compared with the previous results (An & Shi, 2006, 2007; Sun et al., 2013; Deng et al., 2016).

4.2. Thickness of Thermal Lithosphere

The thickness of thermal lithosphere beneath Northeast China (Figure 5) is estimated by considering the isothermal surface at 1300℃ as its lower boundary (Artemieva & Mooney, 2001; An & Shi, 2006, 2007; He, 2014). The average thermal lithosphere thickness in the study region is approximately 100 km, which is consistent with the values determined by the previous studies (Wang, 2001; An & Shi, 2006; Wang & Cheng, 2011). Some small-scale variations in the thermal lithosphere thickness between the different tectonic blocks in Northeast China are revealed. The bottom boundary of the thermal lithosphere on the western and eastern sides of the NSGL changes dramatically, varying from ~80 km to more than 100 km depth. The thinnest thermal lithosphere (~60 km) occurs beneath the Changbai volcanic area. Other Cenozoic volcanic areas such as Longgang, Jingpohu and Halaha also exhibit a thinner thermal lithosphere (~70 km). The thermal lithosphere is relatively thin (~80 km) beneath the central area of the Songliao Basin, the Sanjiang Basin and the Dunhua-Mishan fault. The thermal lithosphere is thick beneath the edge of the Songliao Basin, reaching ~120 km. These results are in good agreement with the thickness of seismic lithosphere obtained by some receiver function studies (Guo et al., 2014; Zhang et al., 2014). Previous studies have shown that the thickness difference between the seismic lithosphere and the thermal lithosphere is small in eastern China (Wang & Cheng, 2011; He, 2014), suggesting that our result is robust.

4.3 Lithospheric Strength Structure

We further estimate the integrated lithospheric strength in Northeast China using the obtained 3-D temperature model (Figure 6). Four east-west vertical cross-sections of the lithospheric strength are shown in Figure 7, which indicate that the lithospheric rheological strength coincides with the major tectonic features. As a whole, the lithosphere beneath the NSGL and the Songliao Basin edge exhibit a high strength (Figure 6). The lithospheric strength is very low beneath some Cenozoic volcanic areas such as Halaha, Abaga and Changbai (Figures 6, 7a and 7d). In addition, the lithospheric strength is generally low beneath some Cenozoic extensional basins, such as the Erlian Basin, the Sanjiang Basin and the central part of the Songliao Basin (Figures 6, 7c and 7d). The lithospheric strength is also low beneath the major fault zones, such as the Solonker-Xar Moron-Changchun-Yanji suture (SXCYS) and the Dunhua-Mishan fault (Figure 6).

Figure 8 shows yield strength envelops beneath six key areas in Northeast China. The upper crust predominantly deforms by frictional sliding, whereas brittle fracture becomes dominant in the upper part of the middle crust and even the lithospheric mantle. Both the Erlian Basin and the Hailar Basin exhibit a stronger middle crust but a very weak lower crust and upper mantle. The lithospheric strength values of the Songliao Basin and the Sanjiang Basin are similar to those of the Erlian Basin. The strength envelops in the Changbai and Halaha volcanic areas are characterized by a much stronger upper crust than the middle crust. A major difference between the strength profiles of the volcanic areas and the extensional basins is the existence of a weak middle crust beneath the volcanic areas. In addition, the ductile regime becomes more dominant in the upper crust beneath the volcanic areas than that beneath the extensional basins. In general, the lithospheric strength is primarily concentrated in the upper and middle crust (Figure 8), indicating that Northeast China deforms according to the “crème brûlée” model. The strength of the lower crust is relatively low, which may imply the presence of decoupling between the crust and the lithospheric mantle. The upper crust and the middle crust with a high rigidity are the major parts that bear the tectonic stress in the lithosphere.

4.4. Lithospheric Strength and Seismicity

Seismicity is a good indicator for active tectonic deformation, because earthquakes are generally caused by brittle fracture of the lithospheric plate. Hence, there should be some links between seismicity and variations of the lithospheric strength. We use the International Seismological Center (ISC) catalog that lists earthquakes occurring in Northeast China during 1970 to 2020 with $M_b \geq 4.0$ to analyze the relationship between the lithospheric strength and crustal seismicity (see Figures 6 and 7). Most of the earthquakes occurred close to both sides of the NSGL where the lithospheric strength is higher or the areas characterized by sharp strength variations. These rigid areas are able to accumulate tectonic stress and liable to rupture under the effect of the stress. There exists a high concentration of crustal earthquakes in the central part of the Songliao Basin where the lithosphere exhibits a higher temperature and a lower rigidity. The crustal fluids would weaken the rocks and then trigger earthquakes (e.g., Mishra & Zhao, 2003; Huang & Zhao, 2004; Wei et al., 2013; Xia et al., 2020; Li et al., 2021). Some earthquakes occurred in the SXCYS and the Tanlu fault zone, which may be attributed to the tectonic stress associated with the strike-slip faulting. Swarms of deep-focus earthquakes (> 400 km depth) occur actively beneath the Wangqing and Hunchun areas in Jilin province, which are located within the subducting Pacific plate (Zhang & Tang, 1983; Zhao & Tian, 2013; Jiang et al., 2015; Chen et al., 2017; Jiang et al., 2019). Most of the earthquakes in Northeast China occurred in the upper and middle crust and are restricted in a depth range of 10-20 km, where the lithospheric strength changes dramatically. In contrast, few earthquakes occurred in the lower crust characterized by a low rigidity, indicating that the lower crust is under a ductile condition.

4.5. Uncertainty Estimates

We also investigate the effect of uncertainties of the 3-D velocity models on the temperature estimation. Although previous studies have indicated that the effect of mantle composition variation on the inverted temperature structure is very small (Nolet and Zielhuis, 1994; Sobolev et al., 1996; Goes et al., 2000), we investigate the relationship between temperature and Vp and Vs computed at 50 km depth for the on-cratonic mantle model (with olivine 83%, orthopyroxene 15% and garnet 2%) proposed by Shapiro & Ritzwoller (2004), as shown in Figure 9. In general, uncertainties in the mantle composition variation in the velocity-temperature (V-T) conversion are less than 1% for both Vp and Vs models, as compared with those from the off-cratonic mantle model (blue lines in Figure 9), which are virtually negligible.

The anelastic parameters may not as well constrained by laboratory measurements as the elastic parameters of mantle minerals. Thus, the anelastic correction would contribute to the major part of uncertainty in the V-T conversion. Referring to Shapiro & Ritzwoller (2004), we investigate the relationship between temperature and Vp and Vs computed at 50 km depth through increasing A by 50% of the anelastic parameters (red lines in Figure 9). The Vp and Vs variations at 1500°C are roughly 2% and 6% respectively, but they are less than 1% at ~1300°C and 1100°C. These results indicate that uncertainties resulting from the anelastic correction are large at high temperatures (> 1500°C), but can be ignored at lower temperatures (< 1100°C).

In this study, the effect of partial melt or the presence of fluids in the upper mantle is not taken into account because it has not been well constrained by experimental results so far, which may cause some uncertainties in the V-T conversion. In addition, the 3-D Vp and Vs models we used also have some uncertainties. The Vp and Vs uncertainties at depths < 120 km are generally smaller than 0.1 km/s, which may cause a temperature variation of 50-130°C. The Vs uncertainties at depths greater than 120 km are mostly < 0.2 km/s, which may cause a temperature variation of 80-150°C. Although the uncertainties may be larger at high temperatures (> 1300°C), they have a negligible effect on the estimation of lithospheric strength because the temperature is well above the value (~900°C) at which the lithospheric strength drops almost to zero (Ranalli, 1994; Jackson et al., 2002).

4.6. Tectonic Implications

Combining the results of this work and many previous studies, we deem that the lithospheric structure under Northeast China is very heterogeneous. The Changbai volcanic area, the central part of the Songliao Basin and the Sanjiang Basin in the eastern side of the NSGL exhibit lower seismic velocity, higher temperature, thinner thermal lithosphere and lower lithospheric strength. In addition, these areas, in particular, the Songliao Basin, exhibit higher heat flows and larger geothermal gradients (Tian et al., 1992; Wang, 2001; Ren et al., 2002; Wang & Cheng, 2011; Xu et al., 2013; Jiang et al., 2016). Hence, we think that the subduction of the (Paleo-) Pacific plate beneath the Eurasian plate since the late Mesozoic has resulted in ascending of wet and hot asthenospheric material in the big mantle wedge (BMW) above the Pacific slab that is stagnant in the mantle transition zone, leading to the long-term thermo-chemical erosion beneath these Cenozoic volcanic areas and extensional basins (e.g., Zhao et al., 2004, 2009; Lei & Zhao, 2005; Zhao & Tian, 2013; Jia et al., 2022). The Tanlu fault system might serve as a channel for the upwelling of the wet and hot asthenospheric material and play an essential role in the destruction and thinning of the lithosphere in Northeast and eastern China during the Late Mesozoic to Cenozoic (e.g., Lei et al., 2020). The persistent thermo-chemical erosion of the upwelling asthenospheric material may induce the delamination of partial lithosphere beneath the Songliao Basin, resulting in a relatively thin thermal lithosphere beneath the central part of the basin. The basin edge is characterized by faster seismic velocity and stronger lithosphere, lower temperature and thicker thermal lithosphere, which may indicate a stable lithosphere that has not been delaminated. These features also suggest the strong lateral heterogeneity of the lithosphere beneath the Songliao Basin. The lithospheric delamination beneath the Songliao Basin might induce upwelling of the surrounding small-scale hot asthenospheric material, providing magmas to the Halaha and Abaga volcanoes in the western side of the NSGL (e.g., Wei et al., 2019; Jia et al., 2022). Hence, prominent high-T zones are visible beneath these areas. Summarizing all these results, we present a cartoon to describe the mantle structure and dynamics under Northeast China and the formation mechanism of the Cenozoic intraplate volcanism (Figure 10).

5. Conclusions

We use high-resolution 3-D P- and S-wave velocity models to investigate the thermal structure of the lithosphere in Northeast China and estimate the thermal lithosphere thickness from the 1300°C isotherm of the mantle adiabatic temperature. A rheological strength model of the lithosphere under Northeast China is also determined. The main results of this work are summarized as follows.

(1) The lithosphere beneath the Changbai volcanic area and the central part of the Songliao Basin is characterized by higher temperature, thinner thermal lithosphere and lower rheological strength, which are caused by the upwelling hot and wet asthenospheric material in the big mantle wedge above the subducting Pacific plate beneath East Asia.

(2) The Songliao Basin edge is characterized by lower temperature, thicker thermal lithosphere and higher rheological strength, indicating that the thermo-chemical erosion of the upwelling asthenospheric material may induce delamination of partial lithosphere under the Songliao Basin, but a relatively stable lithosphere may still remain under the basin edge.

(3) The Halaha and Abaga volcanic areas in the western side of the NSGL exhibit higher temperature, thinner thermal lithosphere and lower rheological strength, which may be caused by small-scale upwelling of hot asthenospheric material associated with the delamination of partial lithosphere beneath the Songliao Basin.

(4) The lithospheric strength is primarily concentrated in the crust beneath Northeast China, suggesting that the study region deforms according to the "crème brûlée" model.

(5) Most of the earthquakes in Northeast China take place in the upper and middle crust, indicating that the upper and middle crust is brittle and so bears the tectonic stress in the lithosphere.

Appendix: Mineral Physics Approach

The density (ρ_0) and elastic moduli (K_0 and μ_0) of common upper mantle minerals at normal temperature and pressure ($T_0 = 300K, P = 0$) can be obtained through laboratory measurements (see Table S4). Then the density and elastic moduli of each mineral at a specific temperature T and zero pressure ($P = 0$) are estimated using the following equations (Anderson, 1988; Duffy & Anderson, 1989; Vacher et al., 1998):

$$\rho(T,0) = \rho_0\, exp\left[-\int_{T_0}^{T} \alpha(T^{'})dT^{'}\right]$$

$$\alpha(T) = a_0 + a_1 T + a_2 T^{-1} + a_3 T^{-2} \tag{A1}$$

$$M(T,0) = M_0 [\frac{\rho(T,0)}{\rho_0}]^{\delta_M}$$

$$\delta_M = -\frac{1}{\alpha M_0}\frac{\partial M}{\partial T} \tag{A2}$$

where ρ_0 and $\rho(T,0)$ are densities of lithospheric minerals at the normal and specific temperatures, respectively, $\alpha(T)$ is the coefficient of thermal expansion (CTE), $a_i (i = 0,1,2,3)$ represents parameters measured at the laboratory (see Table S4), M is elastic modulus, and δ_M is the Anderson-Grüneisen parameter.

Combining the Euler finite strain method and the third-order Birch-Murnaghan isothermal equation of state (Birch, 1947; 1978), we have:

$$P = -3K_{T,0}(1-2\varepsilon)^{5/2}[\varepsilon + \frac{3}{2}(4 - \frac{\partial K}{\partial P})\varepsilon^2] \tag{A3}$$

where ε is the Euler strain that can be calculated by solving Eq. (A3) using the pressure values from the PREM model (Dziewonski & Anderson, 1981). Then the density and elastic moduli of each upper mantle mineral at a specific temperature and pressure can be estimated with the following formulas (Deschamps et al., 2002):

$$\rho(T,P) = \rho(T,0)(1-2\varepsilon)^{3/2} \tag{A4}$$

$$K(T,P) = (1-2\varepsilon)^{\frac{5}{2}}(K_{T,0} + C_K\varepsilon)$$

$$C_K = 5K_{T,0} - 3K_{T,0}\frac{\partial K}{\partial P} \tag{A5}$$

$$\mu(T,P) = (1-2\varepsilon)^{\frac{5}{2}}(\mu_{T,0} + C_\mu\varepsilon)$$

$$C_\mu = 5\mu_{T,0} - 3K_{T,0}\frac{\partial \mu}{\partial P} \tag{A6}$$

In this study, the off-cratonic mantle model (with olivine 68%, orthopyroxene 18%, clinopyroxene 11% and garnet 3%) proposed by Shapiro & Ritzwoller (2004) is adopted, because Northeast China has experienced frequent tectonic events during the late Mesozoic to Cenozoic. The density and elastic moduli of the upper mantle can be calculated using the Voigt-Reuss-Hill method (Watt et al., 1976). Then the P- and S-wave velocities can be determined using the following equations:

$$V_P(T,P) = \sqrt{\frac{\bar{K}(T,P)+\frac{4}{3}\bar{\mu}(T,P)}{\bar{\rho}(T,P)}}$$

$$V_S(T,P) = \sqrt{\frac{\bar{\mu}(T,P)}{\bar{\rho}(T,P)}} \tag{A7}$$

Some previous studies have suggested that seismic velocity can be significantly affected by anelasticity of the mantle as the depth increases (e.g., Karato & Spetzler, 1990; Karato, 1993). The effect of anelasticity on Vs is generally estimated with the quality factor as follows (Anderson & Given, 1982; Goes et al., 2000):

$$Q_S(T,P,\omega) = A\omega^a \, exp\left[\frac{a(H^*+PV^*)}{RT}\right] \tag{A8}$$

where A and a are constants measured at laboratory, ω is frequency, H^* and V^* are activation energy and activation volume, respectively, and R is gas constant. Following Sobolev et al. (1996), we use A=0.148, a=0.15, H^*=500 kJ·mol^{-1}, and V^*=20 cm^3·mol^{-1}. The P-wave quality factor can be expressed as (Anderson & Given, 1982):

$$Q_P(T,P,\omega) = (9/4)Q_S(T,P,\omega) \tag{A9}$$

Thus, considering the anelastic effect, Vp and Vs can be expressed as (Minster & Anderson, 1981; Goes et al., 2000; Cammarano et al., 2003):

$$V_P(T,P,\omega) = V_P(T,P)\left[1 - \frac{2}{9}cot\left(\frac{\pi a}{2}\right)Q_S{}^{-1}(T,P,\omega)\right]$$

$$V_S(T,P,\omega) = V_S(T,P)\left[1 - \frac{1}{2}cot\left(\frac{\pi a}{2}\right)Q_S{}^{-1}(T,P,\omega)\right] \tag{A10}$$

The above-mentioned approach is a forward process, which can be used to invert for the upper mantle temperature distribution with 3-D Vp and Vs models determined by seismic tomography.

Acknowledgements

This work was supported by the National Natural Science Foundation of China (grant No. 41874049), a grant from Japan Society for the Promotion of Science (grant No. 19H01996) and Fundamental Research Funds for the Central Universities in China. We appreciate the helpful discussions with Profs. Pengfei Zhao and Rongqiang Wei. We used the Generic Mapping Tools (GMT) software package (Wessel & Smith, 1998) to plot most of the figures.

Data Availability Statement

The 3-D Vp model of Ma et al. (2018) and the obtained 3-D thermal and rheological strength models of the lithosphere beneath Northeast China are archived on the website: (http://doi.org/10.6084/m9.figshare.19246236). The list of crustal earthquakes ($M_b \geq 4.0$) in Northeast China during 1970 to 2020 is available at the International Seismological Center (http://www.isc.ac.uk/iscbulletin/search/catalogue), which is also archived on the website above. The 3-D Vs model of Shen et al. (2016) is available at the website (http://ciei.colorado.edu/Models).

References

Afonso, J. C., & Ranalli, G. (2004). Crustal and mantle strengths in continental lithosphere: is the jelly sandwich model obsolete? *Tectonophysics*, *394*, 221-232. https://doi.org/10.1016/j.tecto.2004.08.006

An, M., & Shi, Y. (2006). Lithospheric thickness of the Chinese continent. *Physics of the Earth and Planetary Interiors*, *159*, 257-266. https://doi.org/10.1016/j.pepi.2006.08.002

An, M., & Shi, Y. (2007). Three-dimensional thermal structure of the Chinese continental crust and upper mantle. *Science in China*, *50*, 1441-1451. https://doi.org/10.1007/s11430-007-0071-3

Anderson, D. L. (1988). Temperature and pressure derivatives of elastic constants with application to the mantle. *Journal of Geophysical Research*, *93*, 4688-4700. https://doi.org/10.1029/JB093iB05p04688

Anderson, D. L., & Given, J. W. (1982). Absorption band Q model for the earth. *Journal of Geophysical Research*, *87*, 3893-3904. https://doi.org/10.1029/JB087iB05p03893

Artemieva, I. M., & Mooney, W. D. (2001). Thermal thickness and evolution of Precambrian lithosphere: a global study. *Journal of Geophysical Research*, *106*, 16387-16414. https://doi.org/10.1029/2000JB900439

Birch, F. (1947). Finite elastic strain of cubic crystals. *Physical Review*, *71*, 809-824. https://doi.org/10.1103/PhysRev.71.809

Birch, F. (1978). Finite strain isotherm and velocities for single-crystal and polycrystalline NaCl at high pressures and 300°K. *Journal of Geophysical Research*, *83*, 1257-1268. https://doi.org/10.1029/JB083iB03p01257

Burov, E. B. (2011). Rheology and strength of the lithosphere. *Marine and Petroleum Geology*, *28*, 1402-1443. https://doi.org/10.1016/j.marpetgeo.2011.05.008

Byerlee, J. D. (1978). Friction of rocks. *Pure and Applied Geophysics*, *116*, 615-626. https://doi.org/10.1007/BF00876528

Cammarano, F., Goes, S., Vacher, P., & Giardini, D. (2003). Inferring upper-mantle temperatures from seismic velocities. *Physics of the Earth and Planetary Interiors*, *138*, 197-222. https://doi.org/10.1016/S0031-9201(03)00156-0

Chen, C., Zhao, D., Tian, Y., Wu, S., Akira, H., Lei, J., et al. (2017). Mantle transition zone, stagnant slab and intraplate volcanism in Northeast Asia. *Geophysical Journal International*, *209*, 68-85. https://doi.org/10.1093/gji/ggw491

Chi, Q., & Yan, M. (1998). Radioactive elements of rocks in North China platform and the thermal structure and temperature distribution of the modern continental lithosphere. *Chinese Journal of Geophysics*, *41*, 38-48.

Deng, Y., & Tesauro, M. (2016). Lithospheric strength variations in Mainland China: Tectonic implications. *Tectonics*, *35*, 2313-2333. https://doi.org/10.1002/2016TC004272

Deschamps, F., Trampert, J., & Snieder, R. (2002). Anomalies of temperature and iron in the uppermost mantle inferred from gravity data and tomographic models. *Physics of the Earth and Planetary Interiors*, *129*, 245-264. https://doi.org/10.1016/S0031-9201(01)00294-1

Doin, M., & Fleitout, L. (1996). Thermal evolution of the oceanic lithosphere: an alternative view. *Earth and Planetary Science Letters*, *142*, 121-136. https://doi.org/10.1016/0012-821X(96)00082-9

Duffy, T. S., & Anderson, D. L. (1989). Seismic velocities in mantle minerals and the mineralogy of the upper mantle. *Journal of Geophysical Research*, *94*, 1895-1912. https://doi.org/10.1029/JB094iB02p01895

Dziewonski, A. M., & Anderson, D. L. (1981). Preliminary reference Earth model.

Physics of the Earth and Planetary Interiors, *25*, 297-356. https://doi.org/10.1016/0031-9201(81)90046-7

Goes, S., Govers, R., & Vacher, P. (2000). Shallow mantle temperature under Europe from P and S wave tomography. *Journal of Geophysical Research*, *105*, 11153-11169. https://doi.org/10.1029/1999JB900300

Goetze, C., & Evans, B. (1979). Stress and temperature in the bending lithosphere as constrained by experimental rock mechanics. *Geophysical Journal International*, *59*, 463-478. https://doi.org/10.1111/j.1365-246X.1979.tb02567.x

Griffin, W. L., Andi, Z., O'Reilly, S. Y., & Ryan, C. G. (1998). Phanerozoic evolution of the lithosphere beneath the Sino-Korean Craton. *Mantle Dynamics and Plate Interactions in East Asia*, *27*, 107-126. https://doi.org/10.1029/gd027p0107

Guo, Z., Cao, Y., Wang, X., Chen, J. Y., Ning, J., He, W., et al. (2014). Crust and upper mantle structures beneath Northeast China from receiver function studies. *Earthquake Science*, *27*, 265-275. https://doi.org/10.1007/s11589-014-0076-x

Guo, Z., Wang, K., Yang, Y., Tang, Y., Chen, J. Y., & Hung, S.-H. (2018). The origin and mantle dynamics of Quaternary intraplate volcanism in Northeast China from joint inversion of surface wave and body wave. *Journal of Geophysical Research: Solid Earth*, *123*, 2410-2425. https://doi.org/10.1002/2017JB014948

Guo. Z., Chen, J. Y., Ning J, Yang, Y., Afonso, J. C., & Tang, Y. (2016). Seismic evidence of on-going sublithosphere upper mantle convection for intra-plate volcanism in Northeast China. *Earth and Planetary Science Letters, 433,* 31-43. https://doi.org/10.1016/j.epsl.2015.09.035

Han, J., Guo, Z., Liu, W., Hou, H., Liu, G., Han, S., et al. (2018). Deep dynamic process of lithosphere thinning in Songliao basin. *Chinese Journal of Geophysics*, *61*, 2265-2279. https://doi.org/10.6038/cjg2018L0155

He, L. (2014). The Rheological boundary layer and its implications for the difference between the thermal and seismic lithospheric bases of the North China Craton. *Chinese Journal of Geophysics*, *57*, 53-61. https://doi.org/10.6038/cjg20140106

Huang, F., He, L., & Wu, Q. (2015). Lithospheric thermal structure of the Ordos Basin and its implications to destruction of the North China Craton. *Chinese Journal of*

Geophysics, *58*, 3671-3686. https://doi.org/10.6038/cjg20151020

Huang, J., & Zhao, D. (2004). Crustal heterogeneity and seismotectonics of the region around Beijing, China. *Tectonophysics*, *385*, 159-180.

Huang, J., & Zhao, D. (2006). High-resolution mantle tomography of China and surrounding regions. *Journal of Geophysical Research*, *111*, B09305. https://doi.org/10.1029/2005JB004066

Jackson, J. (2002). Strength of the continental lithosphere: time to abandon the jelly sandwich? *GSA Today*, *12*, 4-9. https://doi.org/10.1130/1052-5173(2002)012<0004:SOTCLT>2.0.CO;2

Jia, R., Zhao, D., & Wu, J. (2022). P-wave anisotropic tomography of NE China: insight into lithospheric deformation, mantle dynamics and intraplate volcanism. *Geophysical Journal International*, *229*, 1372-1391. https://doi.org/10.1093/gji/ggab516

Jiang, G., Gao, P., Rao, S., Zhang, L., Tang, X., Huang, F., et al. (2016). Compilation of heat flow data in the continental area of China (4th edition), *Chinese Journal of Geophysics*, *59*, 2892-2910. https://doi.org/10.6038/cjg20160815

Jiang, G., Zhao, D., & Zhang, G. (2015). Detection of metastable olivine wedge in the western Pacific slab and its geodynamic implications. *Physics of the Earth and Planetary Interiors*, *238*, 1-7. https://doi.org/10.1016/j.pepi.2014.10.008

Jiang, J., Chen, Q., & Jiao, L. (2019). Waveform detection and location of deep earthquakes in the subduction zone beneath Northeast China. *Chinese Journal of Geophysics*, *62*, 2930-2945. https://doi.org/10.6038/cjg2019M0210

Kang, D., Shen, W., Ning, J., & Ritzwoller, M. H. (2016). Seismic evidence for lithospheric modification associated with intracontinental volcanism in Northeastern China. *Geophysical Journal International*, *204*, 215-235. https://doi.org/10.1093/gji/ggv441

Karato, S. (1993). Importance of anelasticity in the interpretation of seismic tomography. *Geophysical Research Letters*, *20*, 1623-1626. https://doi.org/10.1029/93GL01767

Karato, S., & Spetzler, H. A. (1990). Defect microdynamics in minerals and solid-state mechanism of seismic wave attenuation and velocity dispersion in the mantle. *Reviews of Geophysics*, *28*, 399-421. https://doi.org/10.1029/RG028i004p00399

Kirby, S. H. (1983). Rheology of the lithosphere. *Reviews of Geophysics*, *21*, 1458-1487. https://doi.org/10.1029/RG021i006p01458

Kirby, S. H., Durham, W. B., & Stern, L. A. (1991). Mantle phase changes and deep-earthquake faulting in subducting lithosphere. *Science*, *252*, 216-225. https://doi.org/10.1126/science.252.5003.216

Kirby, S. H., Stein, S., Okal, E. A., & Rubie, D. C. (1996). Metastable mantle phase transformations and deep earthquakes in subducting oceanic lithosphere, *Reviews of Geophysics*, *34*, 261-306. https://doi.org/10.1029/96RG01050

Kohlstedt, D. L., Evans, B., & Mackwell, S. J. (1995). Strength of the lithosphere: constraints imposed by laboratory experiments. *Journal of Geophysical Research*, *100*, 17587-17602. https://doi.org/10.1029/95JB01460

Laske, G., Masters, G., Ma, Z., & Pasyanos, M. (2013). Update on CRUST1.0 - A 1-degree global model of Earth's crust. *EGU General Assembly Conference Abstracts*.

Lei, J., & Zhao, D. (2005). P-wave tomography and origin of the Changbai intraplate volcano in Northeast Asia. *Tectonophysics*, *397*, 281-295. https://doi.org/10.1016/j.tecto.2004.12.009

Lei, J., Zhao, D., Xu, X., Du, M., Mi, Q., & Lu, M. (2020). P-wave upper-mantle tomography of the Tanlu fault zone in eastern China. *Physics of the Earth and Planetary Interiors*, *299*, 106402. https://doi.org/10.1016/j.pepi.2019.106402

Li, H., Liu, C., Tian, Y., Wu, Z., & Zhu, H. (2021). Seismic tomography of the Songyuan area, Northeast China: constraints on seismogenic structure. *Chinese Journal of Geophysics*, *64*, 1597-1607. https://doi.org/10.6038/cjg2021O0288

Li, S., Weng, A., Li, J., Shan, X., Han, J., Tang, Y., et al. (2020). Deep origin of Cenozoic volcanoes in Northeast China revealed by 3-D electrical structure. *Science China (Earth Sciences)*, *63*, 533-547. https://doi.org/10.1007/s11430-018-9537-2

Li, S., Zhao, G., Dai, L., Liu, X., Zhou, L., Santosh, M., et al. (2012). Mesozoic basins in eastern China and their bearing on the deconstruction of the North China Craton. *Journal of Asian Earth Sciences*, *47,* 64-79. https://doi.org/10.1016/j.jseaes.2011.06.008

Li, Y., Wu, Q., Pan, J., Zhang, F., & Yu, D. (2013), An upper-mantle S-wave velocity model for East Asia from Rayleigh wave tomography. *Earth and Planetary Science Letters*, *377-378*, 367-377. https://doi.org/10.1016/j.epsl.2013.06.033

Liu, J., Han, J., & Fyfe, W. S. (2001). Cenozoic episodic volcanism and continental rifting in Northeast China and possible link to Japan Sea development as revealed from K-Ar geochronology. *Tectonophysics*, *339*, 385-401. https://doi.org/10.1016/S0040-1951(01)00132-9

Liu, S., Wang, L., Gong, Y., Li, C., Li, H., & Han, Y. (2005). Thermal-rheological structure of the lithosphere beneath Jiyang Depression: Its implications for geodynamics. *Science in China Series D (Earth Sciences), 48*, 1569-1584. https://doi.org/10.1360/02YD0286

Ma, J., Tian, Y., Liu, C., Zhao, D., Feng, X., & Zhu, H. (2018). P-wave tomography of Northeast Asia: Constraints on the western Pacific plate subduction and mantle dynamics. *Physics of the Earth and Planetary Interiors, 274*, 105-126. https://doi.org/10.1016/j.pepi.2017.11.003

Meng, Q. (2003). What drove late Mesozoic extension of the northern China-Mongolia tract? *Tectonophysics, 369,* 155-174. https://doi.org/10.1016/S0040-1951(03)00195-1

Menzies, M. A., & Xu, Y. (1998). Geodynamics of the North China Craton. In: Mantle Dynamics and Plate Interactions in East Asia. *American Geophysical Union Geodynamic Series*, *27*, 155-165.

Minster, J. B., & Anderson, D. L. (1981). A model of dislocation controlled rheology for the mantle. *Philosophical Transactions of the Royal Society of London, Series A, Mathematical and Physical Sciences*, *299*, 319–356. https://doi.org/10.2307/36869

Mishra, O. P., & Zhao, D. (2003). Crack density, saturation rate and porosity at the

2001 Bhuj, India, earthquake hypocenter: A fluid driven earthquake? *Earth and Planetary Science Letters*, *212*, 393-405. https://doi.org/10.1016/S0012-821X(03)00285-1

Niu, Y. (2005). Generation and evolution of basaltic magmas: some basic concepts and a new view on the origin of Mesozoic-Cenozoic basaltic volcanism in Eastern China. *Geological Journal of China Universities*, *11*, 9-46.

Paige, C., & Saunders, M. (1982). LSQR: an algorithm for sparse linear equations and sparse least squares. *ACM Transactions on Mathematical Software*, *8*, 43–71. https://doi.org/10.1145/355984.355989

Pan, J., Li, Y., Wu, Q., & Yu, D. (2014). 3-D S-wave velocity structure of crust and upper-mantle beneath the northeast China. *Chinese Journal of Geophysics*, *57*, 2077-2087. https://doi.org/10.6038/cjg20140705

Pauselli, C., Ranalli, G., & Federico, C. (2010). Rheology of the Northern Apennines: lateral variations of lithospheric strength. *Tectonophysics*, *484*, 27-35. https://doi.org/10.1016/j.tecto.2009.08.029

Qiu, N., Xu, W., Zuo, Y., Chang, J., & Liu, C. (2017). Evolution of Meso-Cenozoic thermal structure and thermal-rheological structure of the lithosphere in the Bohai Bay Basin, eastern North China Craton. *Earth Science Frontiers*, *24*: 13-26. https://doi.org/10.13745/j.esf.2017.03.002

Ranalli, G. (1994). Nonlinear flexure and equivalent mechanical thickness of the lithosphere. *Tectonophysics*, *240*, 107–114. https://doi.org/10.1016/0040-1951(94)90266-6

Ranalli, G. (2000). Rheology of the crust and its role in tectonic reactivation. *Journal of Geodynamics*, *30*, 3-15. https://doi.org/10.1016/S0264-3707(99)00024-1

Ranalli, G., & Adams, M. (2013). Rheological contrast at the continental Moho: Effects of composition, temperature, deformation mechanism, and tectonic regime. *Tectonophysics*, *609*, 480-490. https://doi.org/10.1016/j.tecto.2012.10.037

Ranalli, G., & Murphy, D. C. (1987). Rheological stratification of the lithosphere. *Tectonophysics*, *132*, 281-295. https://doi.org/10.1016/0040-1951(87)90348-9

Ren, J., Tamaki, K., Li, S., & Junxia, Z. (2002). Late Mesozoic and Cenozoic rifting and its dynamic setting in Eastern China and adjacent areas. *Tectonophysics*, *344*, 175-205. https://doi.org/10.1016/S0040-1951(01)00271-2

Rudnick, R., McDonough, W., & O'Connell, R. (1998). Thermal structure, thickness and composition of continental lithosphere. *Chemical Geology*, *145*, 395–411. https://doi.org/10.1016/S0009-2541(97)00151-4

Rybach, L., & Buntebarth, G. (1984). The variation of heat generation, density and seismic velocity with rock type in the continental lithosphere. *Tectonophysics*, *103*, 335–344. https://doi.org/10.1016/0040-1951(84)90095-7

Sengor, A. M. C., Natal'in, B. A., & Burtman, V. S. (1993). Evolution of the Altaid tectonic collage and Palaeozoic crustal growth in Eurasia. *Nature*, *364*, 299-307. https://doi.org/10.1038/364299a0

Shapiro, N. M., & Ritzwoller, M. H. (2004). Thermodynamic constraints on seismic inversions. *Geophysical Journal International*, *157*, 1175-1188. https://doi.org/10.1111/j.1365-246X.2004.02254.x

Shen, W., Ritzwoller, M., Kang, D., Kim, Y., Lin, F., & Ning, J. (2016). A seismic reference model for the crust and uppermost mantle beneath China from surface wave dispersion. *Geophysical Journal International*, *206*, 954-979. https://doi.org/10.1093/gji/ggw175

Sobolev, S. V., Zeyen, H., Stoll, G., Werling, F., Altherr, R., & Fuchs, K. (1996). Upper mantle temperatures from teleseismic tomography of French Massif Central including effects of composition, mineral reactions, anharmonicity, anelasticity and partial melt. *Earth and Planetary Science Letters*, *139*, 147-163. https://doi.org/10.1016/0012-821X(95)00238-8

Sun, Y., Dong, S., Zhang, H., Li, H., & Shi, Y. (2013). 3D thermal structure of the continental lithosphere beneath China and adjacent regions. *Journal of Asian Earth Sciences*, *62*, 697-704. https://doi.org/10.1016/j.jseaes.2012.11.020

Tao, K., Liu, T., Ning, J., & Niu, F. (2014). Estimating sedimentary and crustal structure using wavefield continuation: theory, techniques and applications. *Geophysical Journal International*, *197*, 443-457.

https://doi.org/10.1093/gji/ggt515

Tesauro, M., Kaban, M. K., & Cloetingh, S. (2012), Global strength and elastic thickness of the lithosphere. *Global and Planetary Change*, *90-91*, 51-57. https://doi.org/10.1016/j.gloplacha.2011.12.003

Tesauro, M., Kaban, M. K., & Mooney, W. D. (2015). Variations of the lithospheric strength and elastic thickness in North America. *Geochemistry Geophysics Geosystems*, *16*, 2197-2220. https://doi.org/10.1002/2015GC005937

Tian, Y., Zhao, D., Sun, R., & Teng, J. (2009). Seismic imaging of the crust and upper mantle beneath the North China Craton. *Physics of the Earth and Planetary Interiors*, *172*, 169-182. https://doi.org/10.1016/j.pepi.2008.09.002

Tian, Y., Legendre, C. P., Zhou, T., Han, J., Wu, M., Zhao, L., et al. (2017). High resolution anisotropic phase velocity tomography of Northeast China and its implication. *Chinese Journal of Geophysics*, *60*, 1659-1675. https://doi.org/10.6038/cjg20170505

Tian, Y., Ma, J., Liu, C., Feng, X., Liu, T., Zhu, H., et al. (2019). Effects of subduction of the western Pacific plate on tectonic evolution of Northeast China and geodynamic Implications. *Chinese Journal of Geophysics*, *62*, 1071-1082. https://doi.org/10.6038/cjg2019M0061

Tian, Y., Zhu, H., Zhao, D., Liu, C., Feng, X., Liu, T., et al. (2016). Mantle transition zone structure beneath the Changbai volcano: Insight into deep slab dehydration and hot upwelling near the 410 km discontinuity. *Journal of Geophysical Research: Solid Earth*, *121*, 5794-5808. https://doi.org/10.1002/2016JB012959

Tian, Z., Han, P., & Xu, K. (1992). The Mesozoic-Cenozoic East China rift system. *Tectonophysics*, *208*, 341-363. https://doi.org/10.1016/0040-1951(92)90354-9

Vacher, P., Mocquet, A., & Sotin, C. (1998). Computation of seismic profiles from mineral physics: the importance of non-olivine components for explaining the 660 depth discontinuity. *Physics of the Earth and Planetary Interiors*, *106*, 275-298. https://doi.org/10.1016/S0031-9201(98)00076-4

Wang, F., Zhou, X., Zhang, L., Ying, J., Zhang, Y., Wu, F., et al. (2006). Late Mesozoic volcanism in the Great Xing'an Range (NE China): Timing and implications for the dynamic setting of NE Asia. *Earth and Planetary Science Letters, 251*, 179-198. https://doi.org/10.1016/j.epsl.2006.09.007

Wang, J., & Li, C. (2018). Curie point depths in Northeast China and their geothermal implications for the Songliao Basin. *Journal of Asian Earth Sciences, 163,* 177-193. https://doi.org/10.1016/j.jseaes.2018.05.026

Wang, Y. (2001). Heat flow pattern and lateral variations of lithosphere strength in China mainland: constraints on active deformation. *Physics of the Earth and Planetary Interiors, 126,* 121-146. https://doi.org/10.1016/S0031-9201(01)00251-5

Wang, Y., & Cheng, S. (2011). Thermal state and rheological strength of the lithosphere beneath the Eastern China. *Geotectonica et Metallogenia, 35*, 12-23.

Wang, Y., & Wang, J. (1992). Using seismic velocity data to calculate the deep crustal rock heat production-along the Shicheng-Huian profile. *Chinese Science Bulletin, 7*, 633–636.

Watt, J. P., Davies, G. F., & O'Connell R. J. (1976). The elastic properties of composite materials. *Reviews of Geophysics, 14*, 541-563. https://doi.org/10.1029/RG014i004p00541

Weertman, J. (1970). The creep strength of the Earth's mantle. *Reviews of Geophysics, 8*, 145-168. https://doi.org/10.1029/RG008i001p00145

Wei, W., Hammond, J., Zhao, D., Xu, J., Liu, Q., Gu, Y., et al. (2019). Seismic evidence for a mantle transition zone origin of the Wudalianchi and Halaha volcanoes in northeast China. *Geochemistry, Geophysics, Geosystems, 20,* 398-416. https://doi.org/10.1029/2018GC007663

Wei, W., Zhao, D., & Xu, J. (2013). P-wave anisotropic tomography in Southeast Tibet: New insight into the lower crustal flow and seismotectonics. *Physics of the Earth and Planetary Interiors, 222,* 47-57. https://doi.org/10.1016/j.pepi.2013.07.002

Wessel, P., & Smith, W. (1998). New, improved version of generic mapping tools released. *Eos Transactions, American Geophysical Union, 79*, 579. https://doi.org/10.1029/98EO00426

Wu, F., Ye, M., & Zhang, S. (1995). Geodynamic model of the Manzhouli-Suifenhe geoscience transect. *Earth Science-Journal of China University of Geosciences*, *20*, 535-539.

Xia, S., Zhou, P., Zhao, D., & Cao, J. (2020). Seismogenic structure in the source zone of the 1918 M7.5 NanAo earthquake in the northern South China Sea. *Physics of the Earth Planetary Interiors*, *302*, 106472. https://doi.org/10.1016/j.pepi.2020.106472

Xu, M., Li, Y., Hou, H., Wang, C., Gao, R., Wang, H., et al. (2017). Structural characteristics of the Yilan-Yitong and Dunhua-Mishan faults as northern extensions of the Tancheng-Lujiang Fault Zone: New deep seismic reflection results. *Tectonophysics*, *706-707*, 35-45. https://doi.org/10.1016/j.tecto.2017.03.018

Xu, P., & Zhao, D. (2009). Upper-mantle velocity structure beneath the North China Craton: Implications for lithospheric thinning. *Geophysical Journal International*, *177*, 1279-1283. https://doi.org/10.1111/j.1365-246X.2009.04120.x

Xu, W., Pei, F., Wang, F., Meng, E., Ji, W., Yang, D., et al. (2013). Spatial-temporal relationships of Mesozoic volcanic rocks in NE China: Constraints on tectonic overprinting and transformations between multiple tectonic regimes. *Journal of Asian Earth Sciences*, *74*, 167-193. https://doi.org/10.1016/j.jseaes.2013.04.003

Xu, Y. (2007). Diachronous lithospheric thinning of the North China Craton and formation of the Daxin'anling-Taihangshan gravity lineament. *Lithos*, *96*, 281-298. https://doi.org/10.1016/j.lithos.2006.09.013

Yan, D., Tian, Y., Zhao, D., Liu, C., Zhu, H., & Li, H. (2019). Upper mantle temperature structure of the North China Craton. *Physics of the Earth and Planetary Interiors*, *293*, 106269. https://doi.org/10.1016/j.pepi.2019.106269

Yang, B., Liu, W., Wang, X., Li, Q., Wang, J., Zhao, X., et al. (2005). Geophysical characteristics of Daxinganling gravitational gradient zone in the East China and its geodynamic mechanism. *Chinese Journal of Geophysics*, *48*, 86-97. https://doi.org/10.1002/cjg2.631

Yang, S., Xiong, X., Zheng, Y., & Shan, B. (2013). Upper-mantle temperature and lithospheric thickness of North China. *Chinese Journal of Geophysics*, *56*, 3855-3867. https://doi.org/10.6038/cjg20131127

Zang, S., Li, C., & Wei, R. (2002b). The determination of rheological mechanics of lithosphere and the influencing factors on the rheological strength of lithosphere. *Progress in Geophysics*, *17*, 50-60.

Zang, S., Liu, Y., & Ning, J. (2002a). Thermal structure of the lithosphere in North China. *Chinese Journal of Geophysics*, *45*, 51-62. https://doi.org/10.1002/cjg2.216

Zang, S., Wei, R., & Liu, Y. (2005). Three-dimensional rheological structure of the lithosphere in the Ordos and its adjacent area. *Geophysical Journal International*, *163*, 339-356.

Zang, S., Wei, R., & Ning, J. (2007). Effect of brittle fracture on the rheological structure of the lithosphere and its application in the Ordos. *Tectonophysics*, *429*, 267-285. https://doi.org/10.1016/j.tecto.2006.10.006

Zhang, B., Lei, J., Yuan, X., Zhang, G., He, J., & Xu, Q. (2020). Detailed Moho variations under Northeast China inferred from receiver function analyses and their tectonic implications. *Physics of the Earth and Planetary Interiors*, *300*, 106448. https://doi.org/10.1016/j.pepi.2020.106448

Zhang, L., & Tang, X. (1983). The underthrusting movement of the western pacific plate and the deep focus earthquake zone of Northeast China. *Chinese Journal of Geophysics*, *26*, 331-340.

Zhang, L., Liu, Q., & He, L. (2016). The different lithospheric thermal structure of North China Craton and its implications. *Chinese Journal of Geophysics*, *59*, 3618-3626. https://doi.org/10.6038/cjg20161009

Zhang, R., Wu, Q., Sun, L., He, J., & Gao, Z. (2014). Crustal and lithospheric structure of Northeast China from S-wave receiver functions. *Earth and Planetary Science Letters*, *401*, 196-205. https://doi.org/10.1016/j.epsl.2014.06.017

Zhao, D., & Tian, Y. (2013). Changbai intraplate volcanism and deep earthquakes in East Asia: a possible link? *Geophysical Journal International*, *195*, 706-724.

https://doi.org/10.1093/gji/ggt289

Zhao, D., Hasegawa, A., & Horiuchi, S. (1992). Tomographic imaging of P and S wave velocity structure beneath northeastern Japan. *Journal of Geophysical Research*, *97*, 19909-19928. https://doi.org/10.1029/92JB00603

Zhao, D., Hasegawa, A., & Kanamori, H. (1994). Deep structure of Japan subduction zone as derived from local, regional, and teleseismic events. *Journal of Geophysical Research*, *99*, 22313-22329. https://doi.org/10.1029/94JB01149

Zhao, D., Lei, J., & Tang, Y. (2004). Origin of the Changbai volcano in northeast China: Evidence from seismic tomography. *Chinese Science Bulletin*, *49*, 1401-1408. https://doi.org/10.1360/04wd0125

Zhao, D., Tian, Y., Lei, J., Liu, L., & Zheng, S. (2009). Seismic image and origin of the Changbai intraplate volcano in East Asia: Role of big mantle wedge above the stagnant Pacific slab. *Physics of the Earth and Planetary Interiors*, *173*, 197-206. https://doi.org/10.1016/j.pepi.2008.11.009

Zhou, J., & Wilde, S. A. (2013). The crustal accretion history and tectonic evolution of the NE China segment of the Central Asian Orogenic Belt. *Gondwana Research*, *23*, 1365-1377. https://doi.org/10.1016/j.gr.2012.05.012

Zhu, R., Chen, L., Wu, F., & Liu, J. (2011). Timing, scale and mechanism of the destruction of the North China Craton. *Science China (Earth Sciences)*, *54*, 789-797. https://doi.org/10.1007/s11430-011-4203-4

<u>Figure captions</u>:

Figure 1. Surface topography and tectonic settings of Northeast China. The white solid line shows the location of the North-South Gravity Lineament (NSGL). The white dashed lines depict boundaries of major tectonic blocks. The red triangles denote major active volcanoes. The east-west dashed lines denote locations of eight vertical cross-sections shown in Figure 3 and Figure 4. ABGV: Abaga Volcano; HLHV: Halaha Volcano; WDLCV: Wudalianchi Volcano; JPHV: Jingpohu Volcano; LGV: Longgang Volcano; CBV: Changbai Volcano.

Figure 2. Map views of the 3-D temperature structure estimated from a joint inversion of Vp and Vs models. The layer depth is shown at the upper-left corner of each map. The red and blue colors represent high and low temperatures, respectively. The temperature scale is shown below each panel. Other labels are the same as those in Figure 1.

Figure 3. (a-h) East-west vertical cross-sections of the 3-D lithospheric temperature distribution along the eight profiles shown in Figure 1. The black arrow above each panel indicates the location of NSGL, and the red triangles denote major active volcanoes. The black dashed line in each panel depicts the estimated lower boundary of the thermal lithosphere.

Figure 4. The same as Figure 3 but for the 3-D lithospheric temperature distribution obtained by solving the 1-D steady-state heat conduction equation. The black dashed line in each panel depicts the Moho discontinuity.

Figure 5. Distribution of the thermal lithosphere thickness in NE China.

Figure 6. Distribution of the integrated lithospheric strength beneath NE China. The white circles denote epicenters of crustal earthquakes ($M_b \geq 4.0$) occurring during 1970 to 2020, which are listed in the ISC catalog.

Figure 7. (a-d) East-west vertical cross-sections of the lithospheric strength along four profiles. The black dashed line in each panel depicts the Moho discontinuity. The white circles in each panel denote crustal earthquakes ($M_b \geq 4.0$) during 1970 to 2020, which are located within a 50-km width of each profile.

Figure 8. Yield strength envelopes in six key areas of NE China. The dashed lines h1 and h2 in each panel denote the bottom of the upper crust and the middle crust, respectively. BR(a) represents the brittle part where the frictional sliding mechanism is dominant. BR(b) means that the dominant deformation mechanism is brittle fracture. DR represents the ductile part.

Figure 9. Relationship between temperature and P- and S-wave velocities computed for the lithosphere at 50 km depth. The black and blue lines show the results for on-cratonic and off-cratonic mantle models, respectively, with the same anelastic correction. The red lines show the results for the on-cratonic mantle model with a reduced anelastic correction.

Figure 10. A cartoon showing the structure and dynamics of the lithosphere and upper mantle beneath NE China as well as the formation mechanism of Cenozoic intraplate volcanoes (red triangles). The red and purple dots denote crustal earthquakes and deep-focus earthquakes, respectively.

Figure 1.

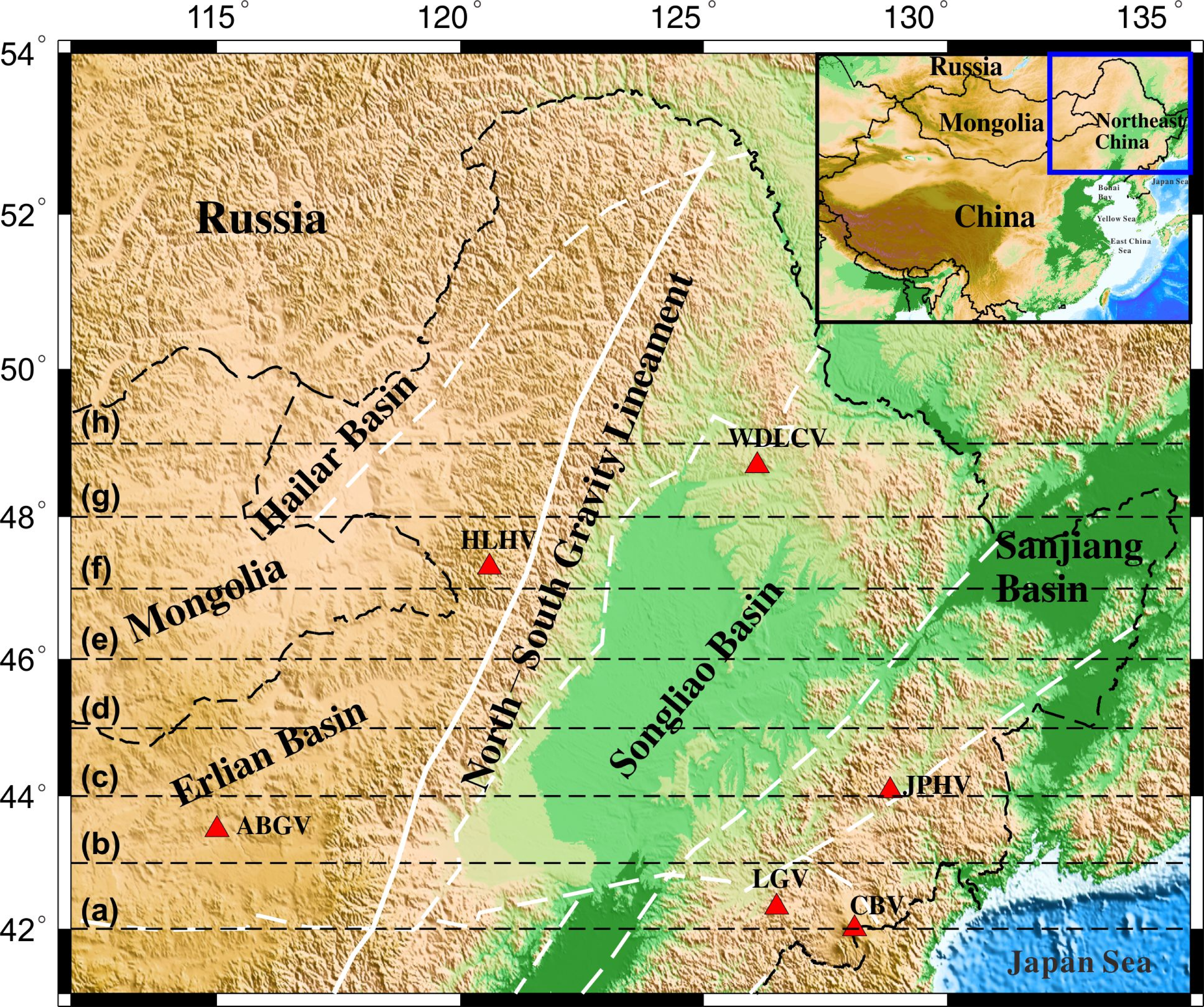

115°
120°
125°
130°
135°
54°
52°
50°
48°
46°
44°
42°
Russia
Mongolia
Northeast China
China
Bohai Bay
Japan Sea
Yellow Sea
East China Sea
Russia
Hailar Basin
North–South Gravity Lineament
Mongolia
Erlian Basin
Songliao Basin
Sanjiang Basin
Japan Sea
WDLCV
HLHV
ABGV
JPHV
LGV
CBV
(h)
(g)
(f)
(e)
(d)
(c)
(b)
(a)

Figure 2.

(a) 50 km
(b) 80 km
(c) 120 km
(d) 160 km
(e) 180 km
(f) 200 km
WDLCV
HLHV
Sanjiang Basin
Songliao Basin
Erlian Basin
JPHV
ABGV
LGV
CBV
112° 116° 120° 124° 128° 132°
54° 52° 50° 48° 46° 44° 42°
1250 1300 1350 1400 1450 1500 1550
1400 1450 1500 1550 1600 1650
1400 1450 1500 1550 1600 1650 1700
1400 1450 1500 1550 1600 1650 1700 1750
1450 1500 1550 1600 1650 1700
1450 1500 1550 1600 1650 1700
Temperature (K)
Temperature (K)

Figure 3.

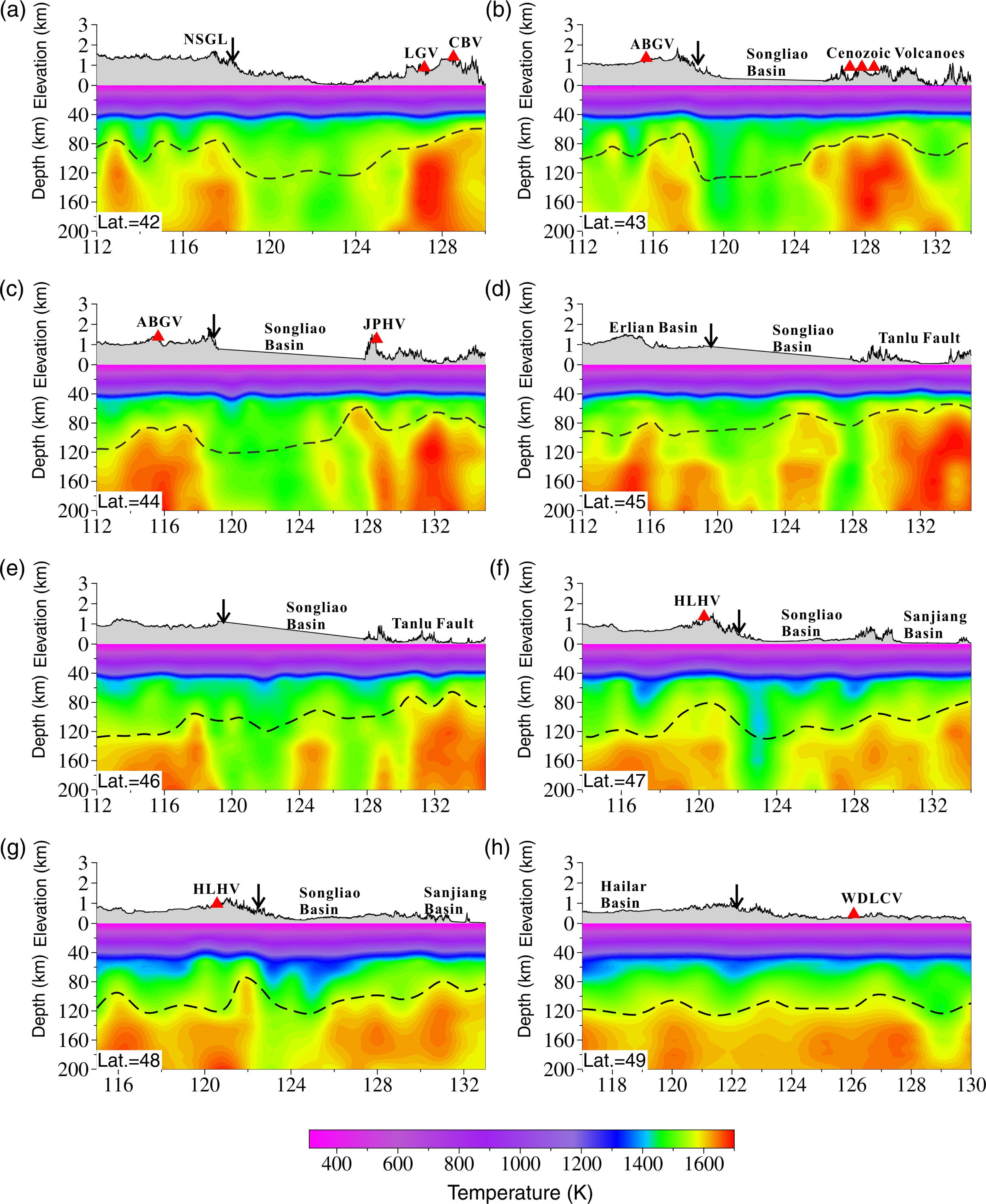

(a)
NSGL
LGV
CBV
Lat.=42
(b)
ABGV
Songliao Basin
Cenozoic Volcanoes
Lat.=43
(c)
ABGV
Songliao Basin
JPHV
Lat.=44
(d)
Erlian Basin
Songliao Basin
Tanlu Fault
Lat.=45
(e)
Songliao Basin
Tanlu Fault
Lat.=46
(f)
HLHV
Songliao Basin
Sanjiang Basin
Lat.=47
(g)
HLHV
Songliao Basin
Sanjiang Basin
Lat.=48
(h)
Hailar Basin
WDLCV
Lat.=49
Elevation (km)
Depth (km)
Temperature (K)

Figure 4.

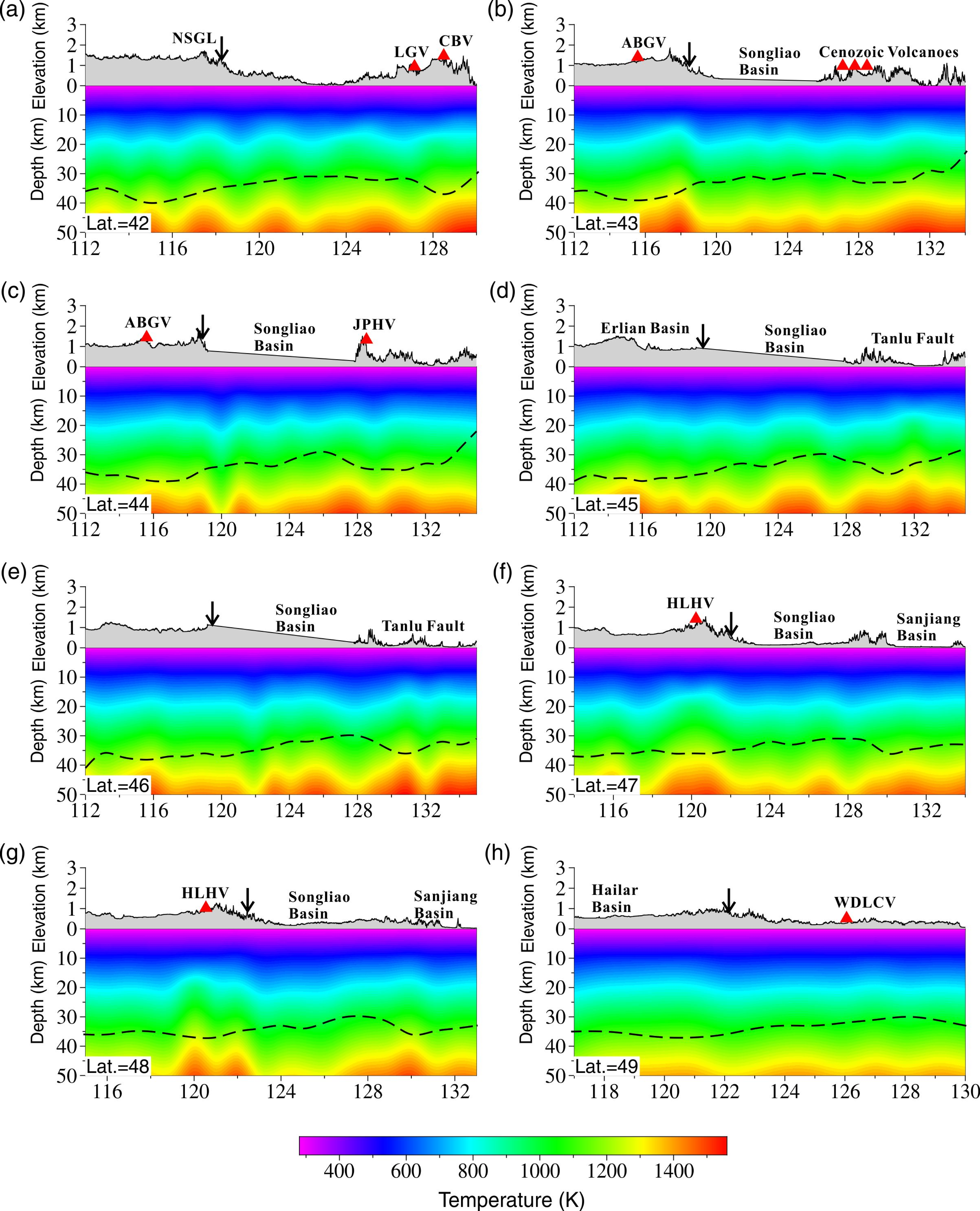

(a)
NSGL
LGV
CBV
Lat.=42
(b)
ABGV
Songliao Basin
Cenozoic Volcanoes
Lat.=43
(c)
ABGV
Songliao Basin
JPHV
Lat.=44
(d)
Erlian Basin
Songliao Basin
Tanlu Fault
Lat.=45
(e)
Songliao Basin
Tanlu Fault
Lat.=46
(f)
HLHV
Songliao Basin
Sanjiang Basin
Lat.=47
(g)
HLHV
Songliao Basin
Sanjiang Basin
Lat.=48
(h)
Hailar Basin
WDLCV
Lat.=49
Elevation (km)
Depth (km)
Temperature (K)

Figure 5.

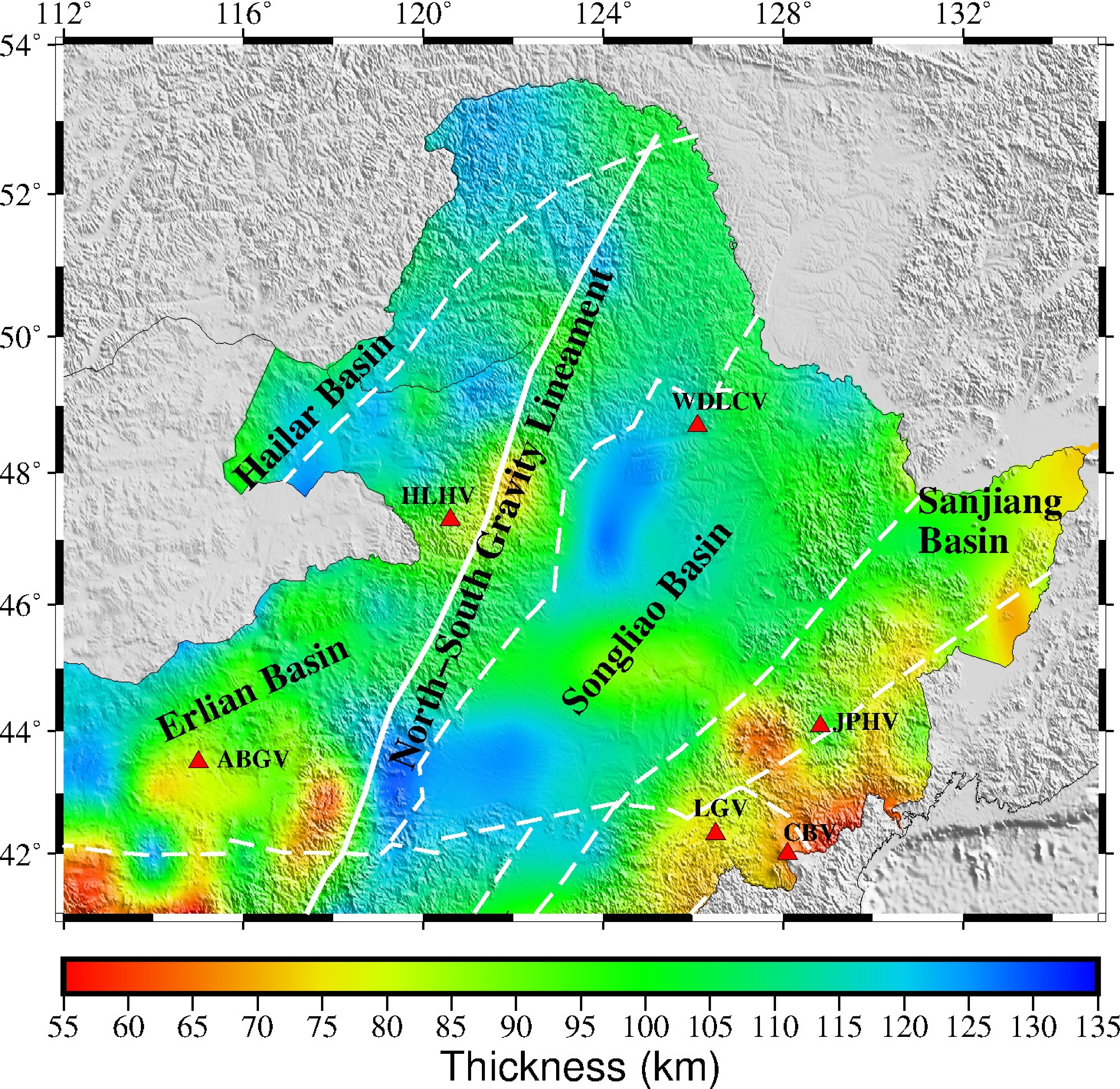
112°
116°
120°
124°
128°
132°
54°
52°
50°
48°
46°
44°
42°
Hailar Basin
North–South Gravity Lineament
WDLCV
HLHV
Sanjiang
Basin
Songliao Basin
Erlian Basin
JPHV
ABGV
LGV
CBV
55
60
65
70
75
80
85
90
95
100
105
110
115
120
125
130
135
Thickness (km)

Figure 6.

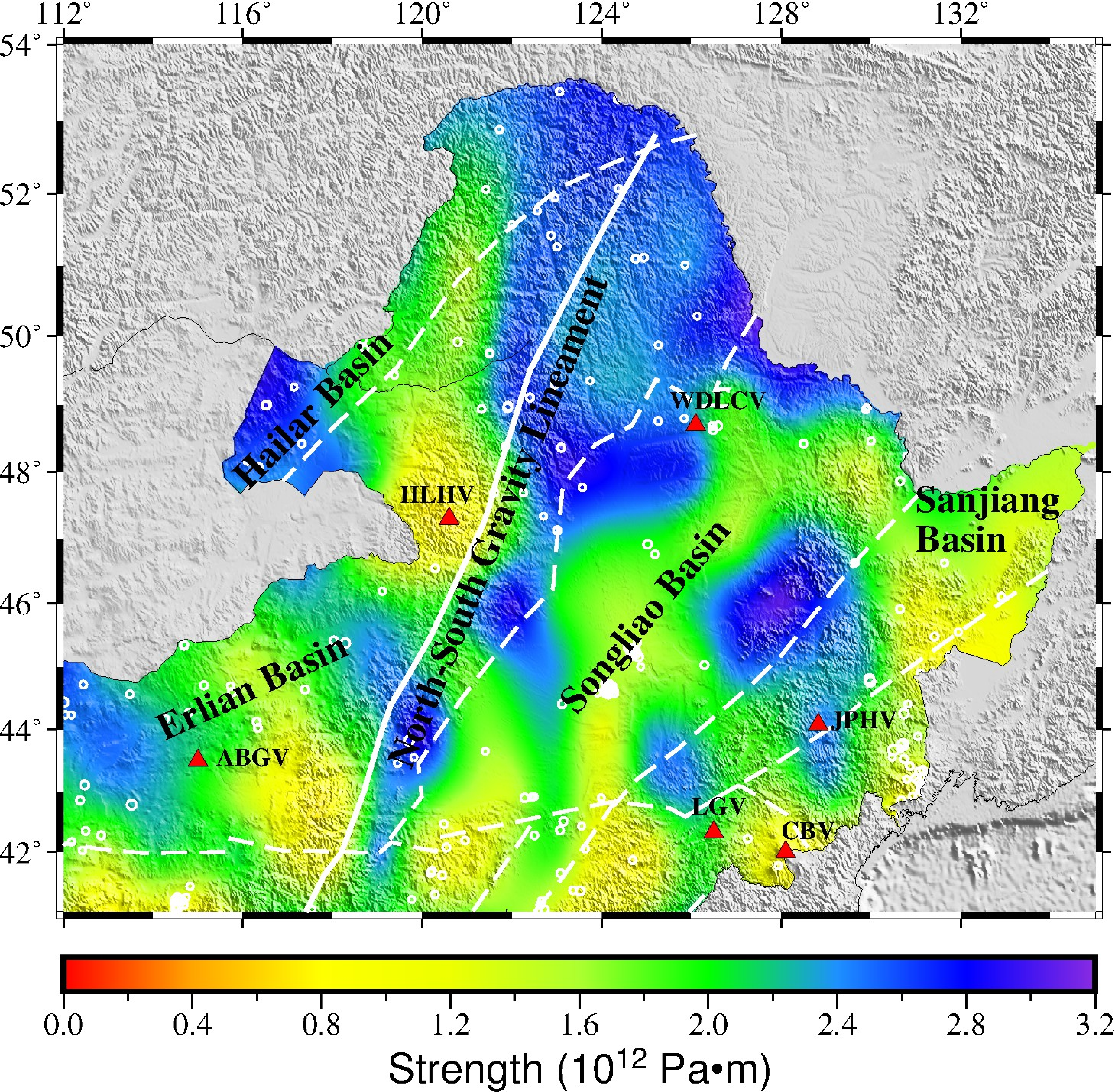
112°
116°
120°
124°
128°
132°
54°
52°
50°
48°
46°
44°
42°
Hailar Basin
North-South Gravity Lineament
WDLCV
HLHV
Sanjiang Basin
Songliao Basin
Erlian Basin
ABGV
JPHV
LGV
CBV
0.0
0.4
0.8
1.2
1.6
2.0
2.4
2.8
3.2
Strength (10^{12} Pa•m)

Figure 7.


(a)
NSGL
LGV
CBV
Elevation (km)
Depth (km)
Lat.=42
(b)
ABGV
JPHV
Songliao Basin
Lat.=44
(c)
Songliao Basin
Tanlu Fault
Lat.=46
(d)
HLHV
Songliao Basin
Sanjiang Basin
Lat.=48
lgσ (MPa)

Figure 8.

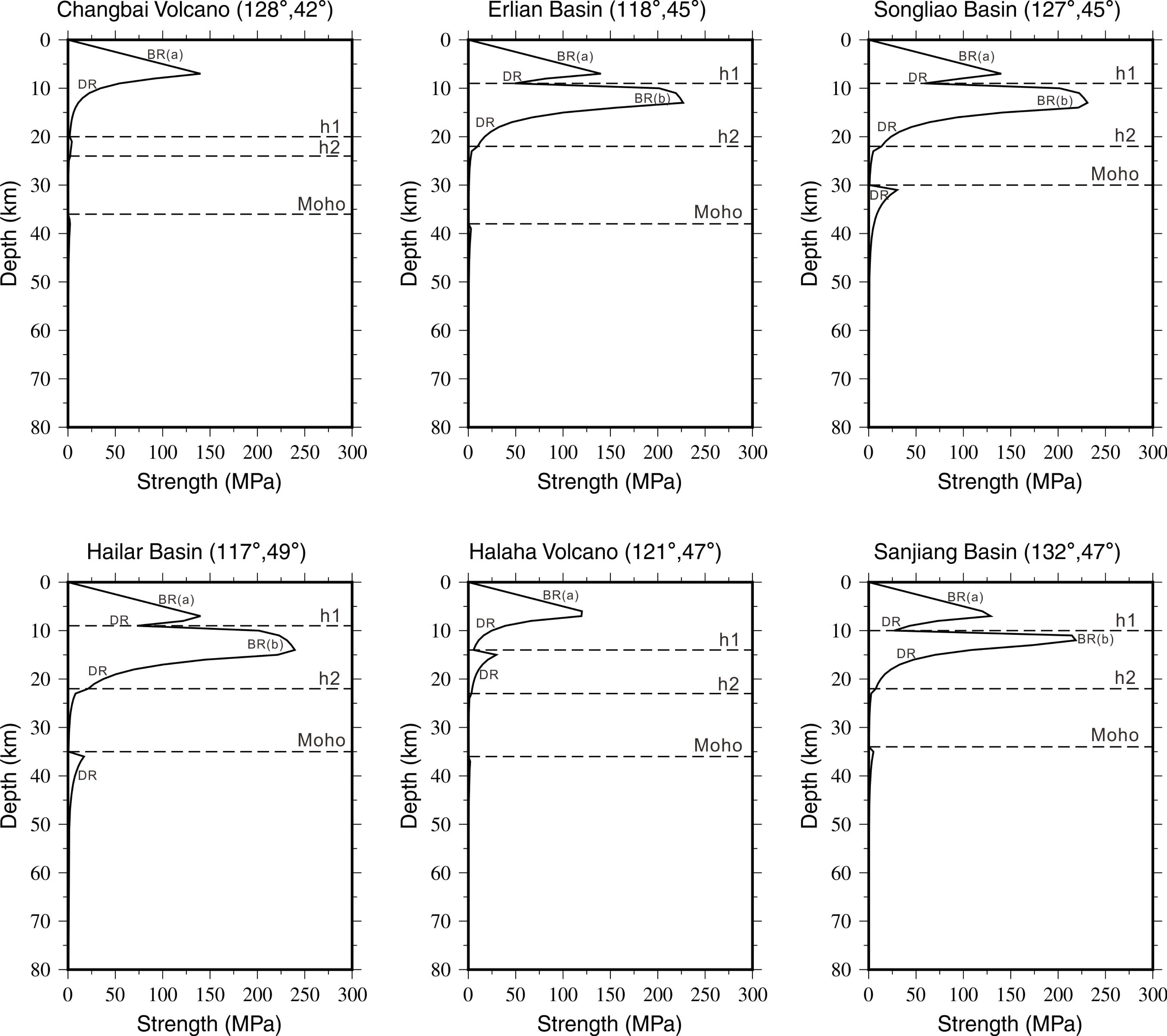
Changbai Volcano (128°,42°)
Erlian Basin (118°,45°)
Songliao Basin (127°,45°)
Hailar Basin (117°,49°)
Halaha Volcano (121°,47°)
Sanjiang Basin (132°,47°)
BR(a)
BR(b)
DR
h1
h2
Moho
Depth (km)
Strength (MPa)
0
10
20
30
40
50
60
70
80
0
50
100
150
200
250
300

Figure 9.

Temperature (˚C)
0
500
1000
1500
9.0
8.5
8.0
7.5
7.0
6.5
6.0
5.5
5.0
4.5
4.0
3.5
3.0
Velocity (km/s)
P-wave velocity
S-wave velocity
on-cratonic composition
off-cratonic composition
on-cratonic composition,modified Q

Figure 10.


54°
52°
50°
48°
46°
44°
42°
112
116
120
124
128
132
HLHV
WDLCV
ABGV
North-South Gravity Lineament
Songliao Basin
JPHV
LGV
CBV
Thermal lithosphere
Asthenosphere
Upwelling
Upwelling
Delamination
410 km
Big Mantle Wedge
Pacific plate
Mantle Transition Zone
Dehydration
660 km
Stagnant slab

Geochemistry, Geophysics, Geosystems

Supporting Information for

Thermal and Rheological Structure of Lithosphere beneath Northeast China

Dong Yan[1], You Tian[1,2*], Dapeng Zhao[3], Hongli Li[1]

1. College of Geoexploration Science and Technology, Jilin University, Changchun 130026, China
2. Changbai Volcano Geophysical Observatory, Ministry of Education, Changchun 130026, China
3. Department of Geophysics, Graduate School of Science, Tohoku University, Sendai 980-8578, Japan

Contents of this file

Figures S1 to S4
Tables S1 to S4

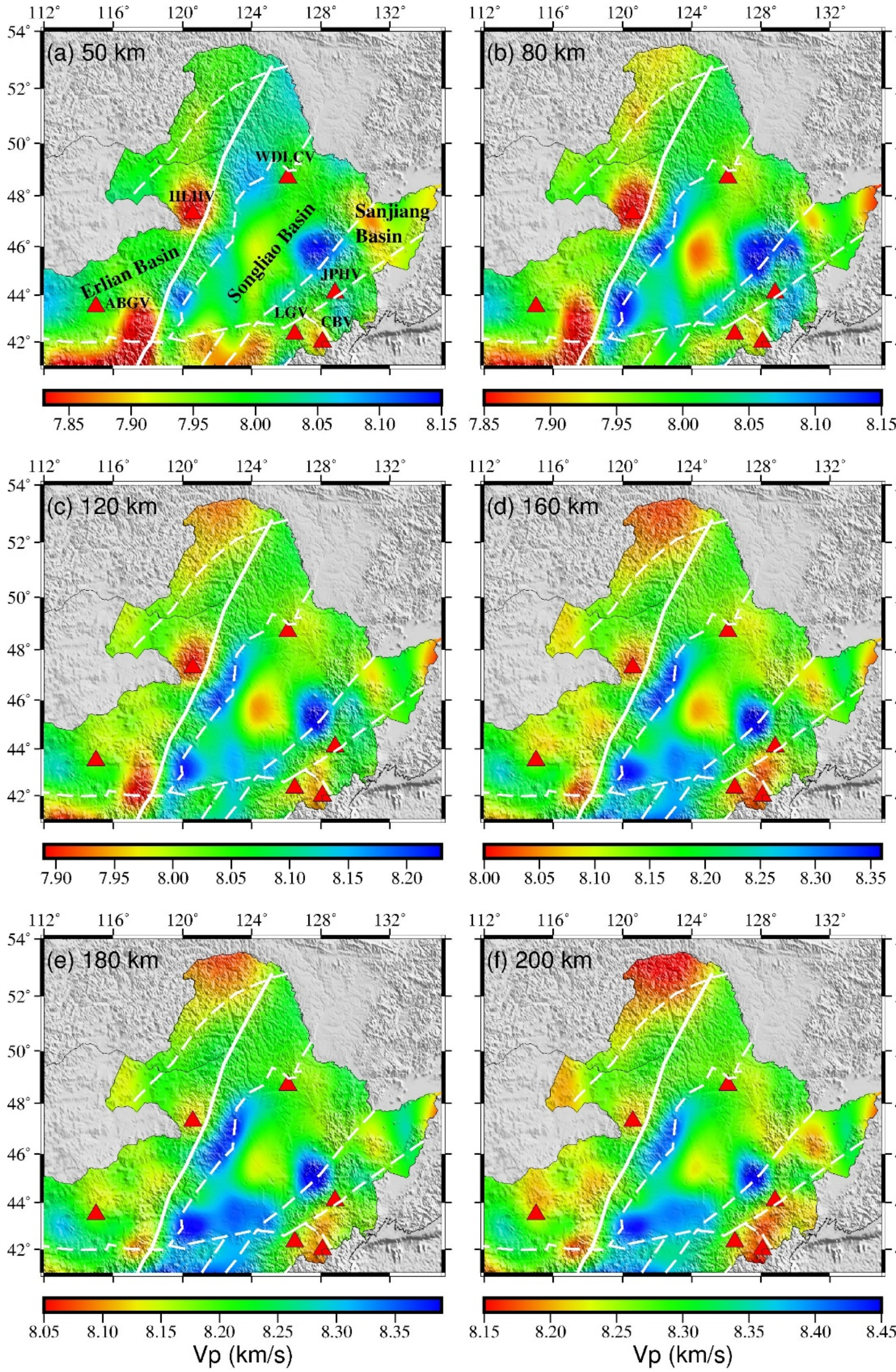

Figure S1. Map views of the 3-D P-wave velocity (Vp) model of Ma et al. (2018). The layer depth is shown at the upper-left corner of each map. The red and blue colors represent low Vp and high Vp, respectively, whose scale is shown below each panel. Other labels are the same as those in Figure 1.

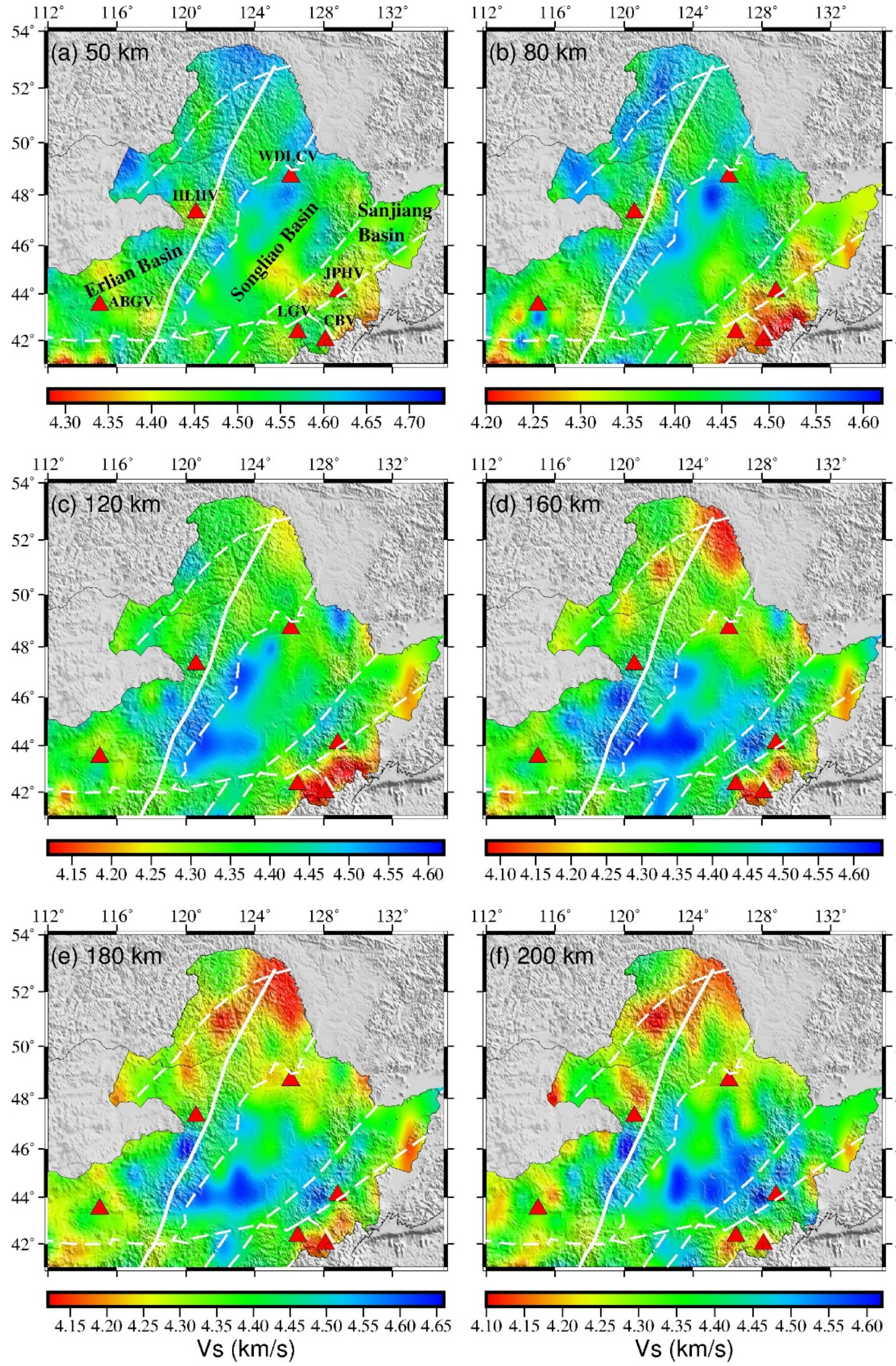

Figure S2. The same as Figure S1 but for the 3-D S-wave velocity (Vs) model of Shen et al. (2016).

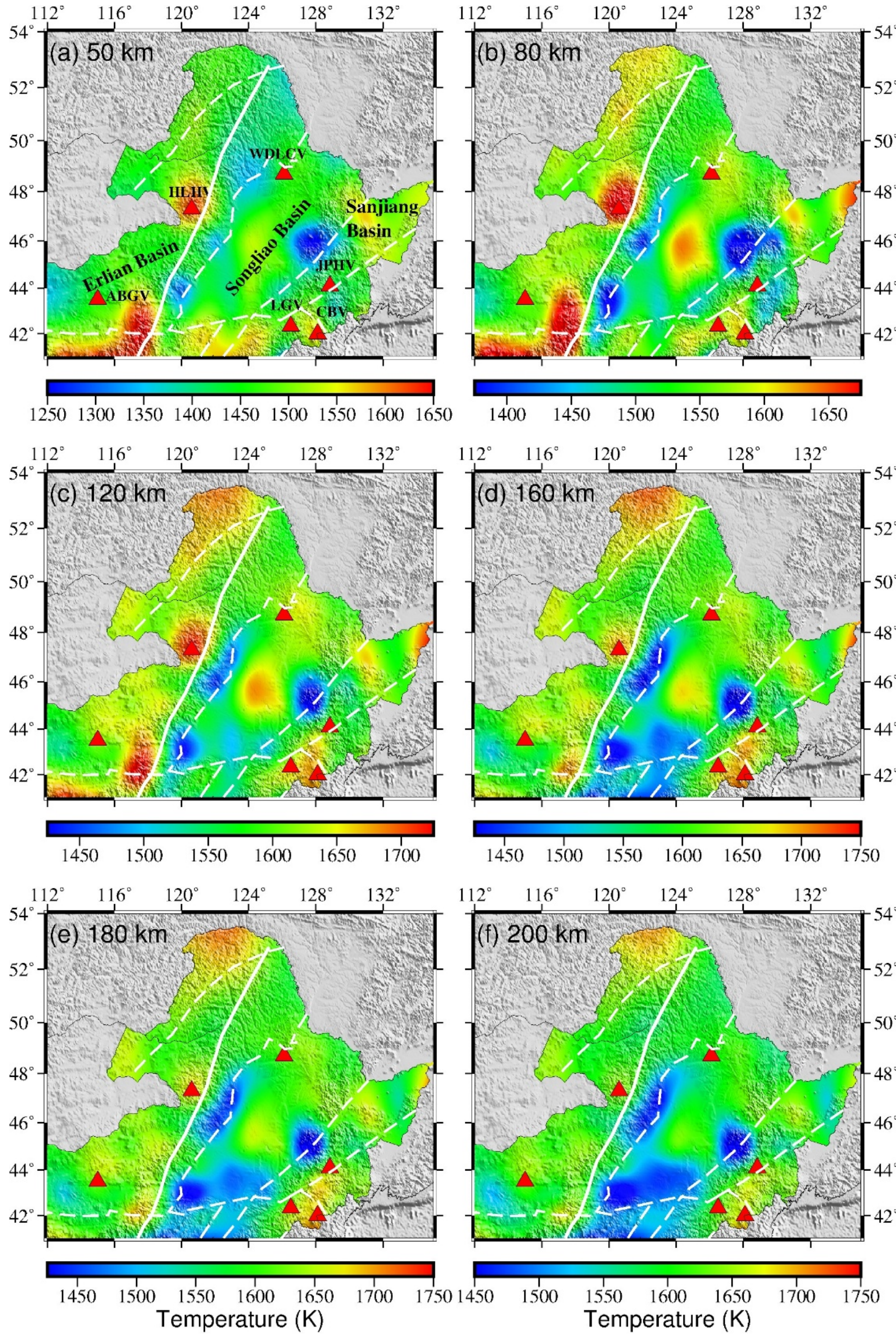

Figure S3. Map views of the temperature image estimated from the 3-D Vp model (Figure S1). The red and blue colors represent high and low temperatures, respectively, whose scale is shown below each panel.

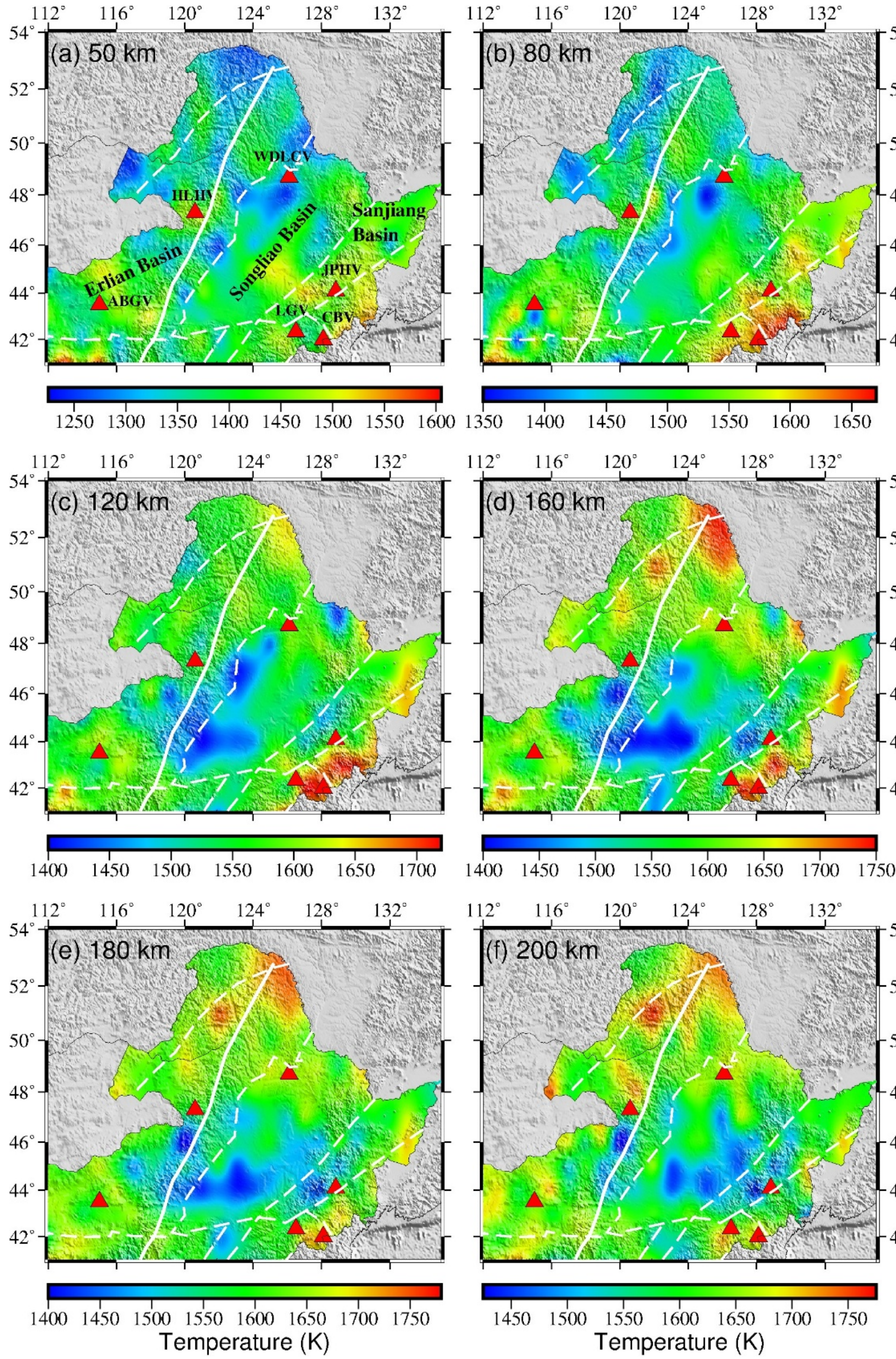

Figure S4. The same as Figure S3 but for the temperature image estimated from the 3-D Vs model (Figure S2).

Table S1. Temperature and pressure derivatives used in the V_P correction formula (compiled from Rybach & Buntebarth, 1984; Wang &Wang, 1992).

Layers	V_P(km·s^{-1})	$\partial V_P/\partial T$(×10^{-4} km·s^{-1}·K^{-1})	$\partial V_P/\partial P$(×10^{-4} km·s^{-1}·MPa^{-1})
Upper crust	< 6.2	-4	4
Middle crust	6.2-6.5	-4	3
Lower crust		-5	3

Table S2. Brittle fracture parameters of several large-scale lithospheric rock samples (compiled from Zang et al., 2007).

Rocks	B_0(MPa)	K	m	α	β	γ
Granite	34.1	4.57	0.52	-1.128	1.732	0.035
Gabbro	36.1	3.18	0.55	-2.536	2.340	0.035
Basalt	48.5	2.98	0.51	-2.536	2.340	0.035
Peridotite	28.3	3.35	0.68	-1.875	1.310	0.035

Table S3. Creep parameters for lithospheric rocks used in this study (compiled from Wang, 2001; Zang et al., 2002b; Liu et al., 2005; Qiu et al., 2017).

Layers	Lithology	ρ(g·cm^{-3})	C(MPa^{-n}·s^{-1})	n	Q (kJ·mol^{-1})
Upper crust	Granite	2.7	1.8×10^{-9}	3.2	123
Middle crust	Anorthosite	2.83	3.2×10^{-4}	3.2	238
Lower crust	Felsic granulite	2.95	8.0×10^{-3}	3.1	243
Lithospheric mantle	Wet peridotite	3.30	2.0×10^{3}	4.0	471

Table S4. Elastic parameters of common upper mantle minerals adopted for this study (compiled from Duffy & Anderson, 1989; Goes et al., 2000).

Mineral	Unit	Olivine	Orthopyroxene	Clinopyroxene	Garnet
ρ	g/cm^3	3.222	3.198	3.280	3.565
K	GPa	129	111	105	173
μ	GPa	82	81	67	92
$\partial K/\partial P$		4.2	6.0	6.2	4.9
$\partial \mu/\partial P$		1.4	2.0	1.7	1.4
$\partial K/\partial T$	MPa/K	-16	-12	-13	-21
$\partial \mu/\partial T$	MPa/K	-14	-11	-10	-10
a_0	$10^{-4}K^{-1}$	0.2010	0.3871	0.3206	0.0991
a_1	$10^{-7}K^{-2}$	0.1390	0.0446	0.0811	0.1165
a_2	10^{-2}	0.1627	0.0343	0.1347	1.0624
a_3	K	-0.3380	-1.7278	-1.8167	-2.5000